Geomorphology 234 (2015) 133–150

Contents lists available at ScienceDirect

Geomorphology

journal homepage: www.elsevier.com/locate/geomorph

Late Quaternary uplift rate inferred from marine terraces, Muroto Peninsula, southwest Japan: Forearc deformation in an oblique subduction zone

Tabito Matsu'ura *,[1]

Japan Nuclear Energy Safety Organization (JNES), Toranomon Towers Office, 4-1-28, Toranomon, Minato-ku, Tokyo 105-0001, Japan

ARTICLE INFO

Article history:
Received 16 July 2014
Received in revised form 9 January 2015
Accepted 17 January 2015
Available online 24 January 2015

Keywords:
Late Quaternary
Marine terrace
Muroto–Misaki (Cape Muroto)
Uplift rate
Southwestern Japan
Oblique subduction zone

ABSTRACT

Tectonic uplift rates across the Muroto Peninsula, in the southwest Japan forearc (the overriding plate in the southwest Japan oblique subduction zone), were estimated by mapping the elevations of the inner edges of marine terrace surfaces. The uplift rates inferred from marine terraces M1 and M2, which were correlated by tephrochronology with marine isotope stages (MIS) 5e and 5c, respectively, include some vertical offset by local faults but generally decrease northwestward from 1.2–1.6 m ky^{-1} on Cape Muroto to 0.3–0.7 m ky^{-1} in the Kochi Plain. The vertical deformation of the Muroto Peninsula since MIS 5e and 5c was interpreted as a combination of regional uplift and folding related to the arc-normal offshore Muroto–Misaki fault. A regional uplift rate of 0.46 m ky^{-1} was estimated from terraces on the Muroto Peninsula, and the residual deformation of these terraces was attributed to fault-related folding. A mass-balance calculation yielded a shortening rate of 0.71–0.77 m ky^{-1} for the Muroto Peninsula, with the Muroto–Misaki fault accounting for 0.60–0.71 m ky^{-1}, but these rates may be overestimated by as much as 10% given variations of several meters in the elevation difference between the buried shoreline angles and terrace inner edges in the study area. A thrust fault model with flat (5–10° dip) and ramp (60° dip) components is proposed to explain the shortening rate and uplift rate of the Muroto–Misaki fault since MIS 5e. Bedrock deformation also indicates that the northern extension of this fault corresponds to the older Muroto Flexure.

1. Introduction

Forearc deformation in oblique subduction zones is not simple because its strain distribution reflects both arc-parallel and arc-normal components of the plate motion. In theory, the forearc forms a sliver (microplate) bounded by a strike–slip fault that accommodates the arc-parallel component of the plate motion (Fitch, 1972). However, if the slip rate on the strike–slip fault is less than its share of the plate motion rate, the forearc sliver may undergo internal deformation to compensate for the slip deficit. In such a case, the forearc sliver does not behave as a rigid microplate and may undergo arc-parallel deformation (McCaffrey, 1992), resulting in arc-parallel strike–slip faults or arc-normal dip–slip faults accompanied by folds. For example, the 2004 Sumatra–Andaman earthquake (M_w 9.3) was generated by pure dip–slip thrust faulting (Lay et al., 2005; Okal, 2007), and the arc-parallel component of the overall oblique plate motion remained to be compensated by slip on a strike–slip fault within the Sumatra–Andaman arc or by arc-parallel forearc deformation. Therefore, in forearc deformation studies and for seismic hazard evaluation in oblique subduction zones, it is important to understand the interplay between interplate megathrust faults and upper-plate faults.

Since the disastrous Tonankai earthquake of 1944 and Nankai earthquake of 1946 (M_w 8.1 and 8.4, respectively), coseismic and short-term deformations in the southwest Japan oblique subduction zone have been the subject of intensive research in connection with expected future large earthquakes (e.g., Central Disaster Prevention Council, 2013; Headquarter of Earthquake Research Project, 2013) (Fig. 1a, b). In the subduction zone, the forearc coastline is characterized by several capes with arc-normal axes, including Capes Ashizuri, Muroto, and Shiono (Fig. 1). In particular, Cape Muroto extends far into the Pacific and is situated on an anticline related to offshore faults (Fig. 2a; Okamura, 1990).

Permanent coastal uplift often results from local thrust faulting and folding within the upper plate (McCalpin and Carver, 2009). For example, local thrust faulting within the upper plate associated with the 1964 Alaska megathrust earthquake caused large amounts of uplift, but the recurrence interval of such local events is probably longer than the interval between megathrust events (Plafker, 1972, 1987). Therefore, long-term deformation of the forearc related to upper-plate structures is also fundamental to understanding the accumulation and distribution of strain in subduction zones.

* Tel.: +81 3 5114 2226; fax: +81 3 5114 2236.
E-mail address: tabito_matsuura@nsr.go.jp.
[1] Now at Regulatory Standard and Research Department, Secretariat of Nuclear Regulation Authority (S/NRA/R), 1-9-9 Roppongi, Minato-ku, Tokyo 106-8450, Japan.

http://dx.doi.org/10.1016/j.geomorph.2015.01.012

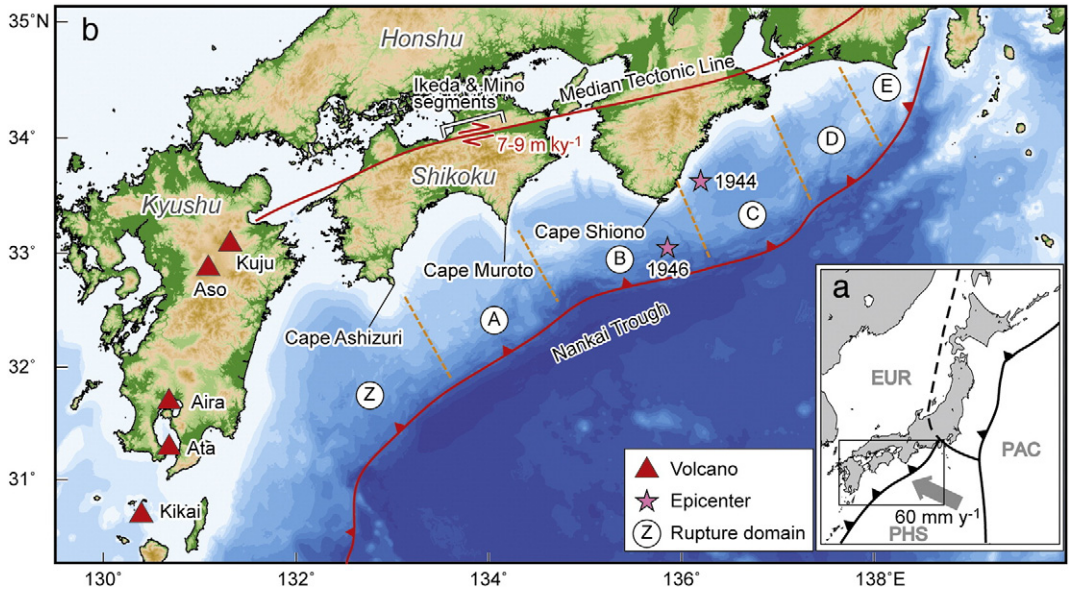

Fig. 1. Location maps showing the southwest Japan forearc. (a) Inset showing the tectonic setting of the southwest Japan arc and the outline of map (b). The Pacific plate (PAC) and Philippine Sea plate (PHS) are subducting under the Eurasia plate (EUR). Lines show plate boundaries (dashed is inferred). Arrows on the lines show plate convergence. (b) Southwest Japan subduction zone. Areas Z, A, B, C, D, and E are rupture segments of interplate earthquakes (Ando, 1975; Yonekura, 1975). Epicenters of the 1944 Tonankai and 1946 Nankai earthquakes are from Headquarter of Earthquake Research Project (2013). Strike–slip rate on the Median Tectonic Line is from Research Group for Active Faults of Japan (1991).

To evaluate offshore fault activity, it is essential to compare short-term deformations with long-term (geologic) deformation data (e.g., Plafker, 1972; Matsu'ura et al., 2009). Long-term deformation data across the southwest Japan forearc have been inferred from late Quaternary marine terraces (Yoshikawa et al., 1964) (Fig. 1a). The deformation of a terrace in a fault-related fold provides critical information for determining the amount of displacement due to the fault. Excess-area analyses, which balance cross-sectional areas of crustal deformation (shortening amount × depth) and use fluvial terrace deformation as a proxy for growth strata, have been useful for determining the slip magnitude on blind thrust faults (e.g., Lave and Avouac, 2000; Bernard et al., 2007; Matsu'ura and Kimura, 2010). The technique can be applied to assess slip on offshore faults by using dated marine terraces, although the age of a marine terrace is generally poorly constrained. Cryptotephras (concentrations of tephra-derived grains in sediments that are not visible as layers; Lowe, 2011), which are powerful age indicators and which have recently been detected in weathered sediments on the Muroto Peninsula (Matsu'ura et al., 2011), offer a promising means for dating late Quaternary marine terraces. In turn, the use of well-dated marine terraces to assess offshore fault activity has global applicability as a tool for helping to assess seismic and tsunami hazards in oblique subduction zones such as the Alaska–Aleutian, Nankai–Ryukyu, Philippine, Andaman–Java–Sumatra, and Hikurangi subduction zones.

This paper reports the late Quaternary deformation rate of the southwest Japan forearc across the Muroto Peninsula, in the southwest Japan subduction zone (Fig. 2a). First, tephrostratigraphy was used to estimate marine terrace ages, and then uplift rates were estimated from the elevation differentials between the inner edges of terrace surfaces and the corresponding eustatic paleo-sea levels. Next, more accurate uplift rates were estimated from the relative heights of the shoreline angle (the intersection between the gently sloping wave-cut platform and the steep sea cliff) and eustatic sea levels during marine isotope stages (MISs) 5e and 5c. Sediment cores obtained from the inner edges of two marine terraces were used to evaluate the thickness of their cover sediments and determine accurate elevations of the buried shoreline angles. Finally, the shortening rate for the Muroto Peninsula was calculated and then divided into two components, the rate for the offshore Muroto–Misaki thrust fault east of Cape Muroto, newly named in this paper, and a rate for other local faults. The geometry and location of the Muroto–Misaki fault were also estimated and its slip rate was calculated.

2. Setting

2.1. Geodynamics and geology

The southwest Japan arc is characterized by the convergence of the Philippine Sea and Eurasia plates at a rate of about 60 mm y^{-1} at the Nankai Trough (Fig. 1a; Seno et al., 1996). The subduction zone is divided into segments corresponding to historical ruptures since AD 684 (Ando, 1975; Yonekura, 1975), labeled Z, A, B, C, D, and E in Fig. 1a. The 1944 Tonankai and 1946 Nankai earthquakes were produced by ruptures on segments C + D and Z (eastern part) + A + B, respectively. Although the Philippine Sea plate is subducting obliquely under the Eurasia plate, the P-axis direction of large earthquakes is not oblique but is partitioned into an arc-normal (NNW–SSE trending) component within the subducting Philippine Sea plate (>20 km depth) and an arc-parallel (ESE–WNW trending) component within the upper crust of the overriding plate (<20 km depth) (Kimura, 2001).

The surface geology of the study area consists of the Shimanto Supergroup (Oligocene to Miocene), the Tonohama Group (Pliocene), terrace deposits (Pleistocene), and Holocene alluvium (Taira et al., 1980; Iwai et al., 2006; Matsu'ura et al., 2011). The Shimanto Supergroup is distributed throughout the Muroto Peninsula (Fig. 2b) and consists of consolidated mudstone. The Tonohama Group commonly underlies terrace deposits, and is composed mainly of sand and gravel with marine mollusk fossils and microfossils, plus terrestrial sediments that include lignite (Iwai et al., 2006). The terrace deposits that are distributed along the current coastline are composed of gravel, sand, and silt, but they do not contain any fossils. Most of them are interpreted as marine sediments because of their coastal distribution and the presence of well-sorted rounded gravel clasts. Some terrace deposits located at river mouths include poorly sorted gravel, probably deposited by fluvial processes (Yoshikawa et al., 1964). Paleosols in the terrace deposits include

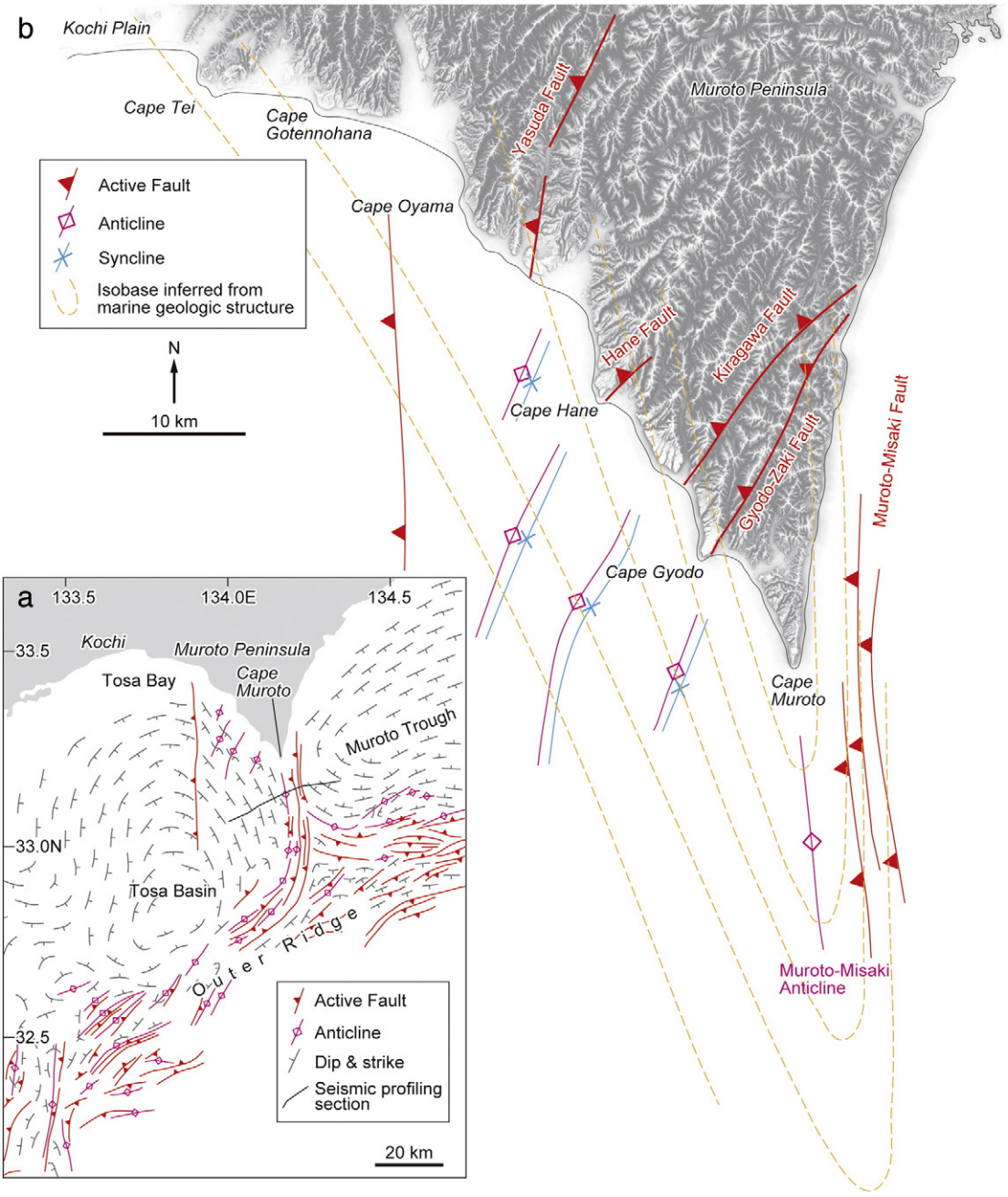

Fig. 2. Location maps showing the outer arc of the Nankai Trough and the Muroto Peninsula (study area) on Shikoku Island. (a) Structural map of Pleistocene sequences in the Muroto Trough and Tosa Basin (Okamura, 1990). Seismic profiling line (black) is also shown. (b) Active faults and folds on land and offshore of the Muroto Peninsula. Active faults on the peninsula are from Research Group for Active Faults of Japan (1991). Offshore active faults and folds are from Okamura (1990).

cryptotephras, such as quartz grains of the Kikai-Tozurahara tephra (MIS 5c–5b, ca. 95 ka) and glass shards of the Aira-Tn (28 ka) and Kikai-Akahoya (7 ka) tephras, all originating from volcanoes on Kyushu Island (Matsu'ura et al., 2011). No Quaternary volcano exists on Shikoku Island.

2.2. Active faults and folds

Active faults running WSW–ENE are well developed on the outer ridge, parallel to the Nankai Trough (Okamura, 1990; Fig. 2a). However, near Cape Muroto they curve to trend N–S (subperpendicular to the trough). Cape Muroto is situated on a N–S-trending anticline (Muroto–Misaki anticline hereafter) that is fringed on its eastern margin by a swarm of offshore thrust faults (Muroto–Misaki fault hereafter) interpreted in seismic profiles (Okamura and Kamishima, 1986; Okamura, 1990; Fig. 2b). Cape Muroto is noted for its well-developed marine terraces, and the MIS 5e terrace on the cape, which reaches 186 m a.s.l. (Yoshikawa et al., 1964: see below), is higher than the corresponding terraces on Cape Shiono (60–69 m a.s.l.) and Cape Ashizuri (70 m a.s.l.) (Koike and Machida, 2001). Because the plate motion rate does not vary along the Nankai Trough, the uplift value is expected to increase offshore. Therefore, the uplift at Cape Muroto should be less than that at Cape Shiono, which is located closer to the Nankai Trough. However, the elevations of the MIS 5e terrace on Capes Shiono and Muroto do not correlate with distance from the trough. This discrepancy indicates that the classic interpretation of Cape Muroto, an accumulation of vertical deformation due to interplate megathrust faulting (e.g., Yoshikawa et al., 1964), should be reconsidered. Okamura (1990) suggested that the local uplift of Cape Muroto might be due to deformation of the Muroto–Misaki anticline. In addition, sessile marine organisms of Holocene age have been raised

above sea level on the Muroto–Misaki anticline, indicating abrupt uplift events associated with large earthquakes (Maemoku, 2006). Large earthquakes, with coastal uplift on the order of 1 m, have occurred with a recurrence interval of 1000–2000 years on offshore faults such as the Muroto–Misaki fault in this area. This recurrence interval is much longer than that of megathrust events (Maemoku, 1988, 2006).

The Median Tectonic Line, a major strike–slip fault, runs the length of Shikoku Island (Fig. 1b). Its slip corresponds to the arc-parallel component of the motion of the Philippine Sea plate, but its late Quaternary slip rate on the Ikeda and Mino segments is 7–9 m ky^{-1}, which is no more than 32–41% of the expected rate (22 m ky^{-1} or more: Kimura, 2002). Active faults on the Muroto Peninsula, inferred from the distribution of vertical offsets on terrace inner edges (Yoshikawa et al., 1964), trend NNE–SSW (Research Group for Active Faults of Japan, 1991; Fig. 2b). Some of them may extend beyond the peninsula to offshore folds (Okamura and Kamishima, 1986).

2.3. Late Quaternary terraces and their distribution

On the Muroto Peninsula, marine and fluvial terrace surfaces are present at multiple levels (Fig. 3; Yoshikawa et al., 1964). Terraces are classified as lower terraces (L), Muroto–Misaki terraces (M3, M2, and M1), and Hane-Saki terraces (H2 and H1) in ascending order. The M1 terrace has been assigned to MIS 5e because it has the widest distribution and probably corresponds to the highest sea level (Yoshikawa et al., 1964). Furthermore, the terrace deposits, which are overlain by

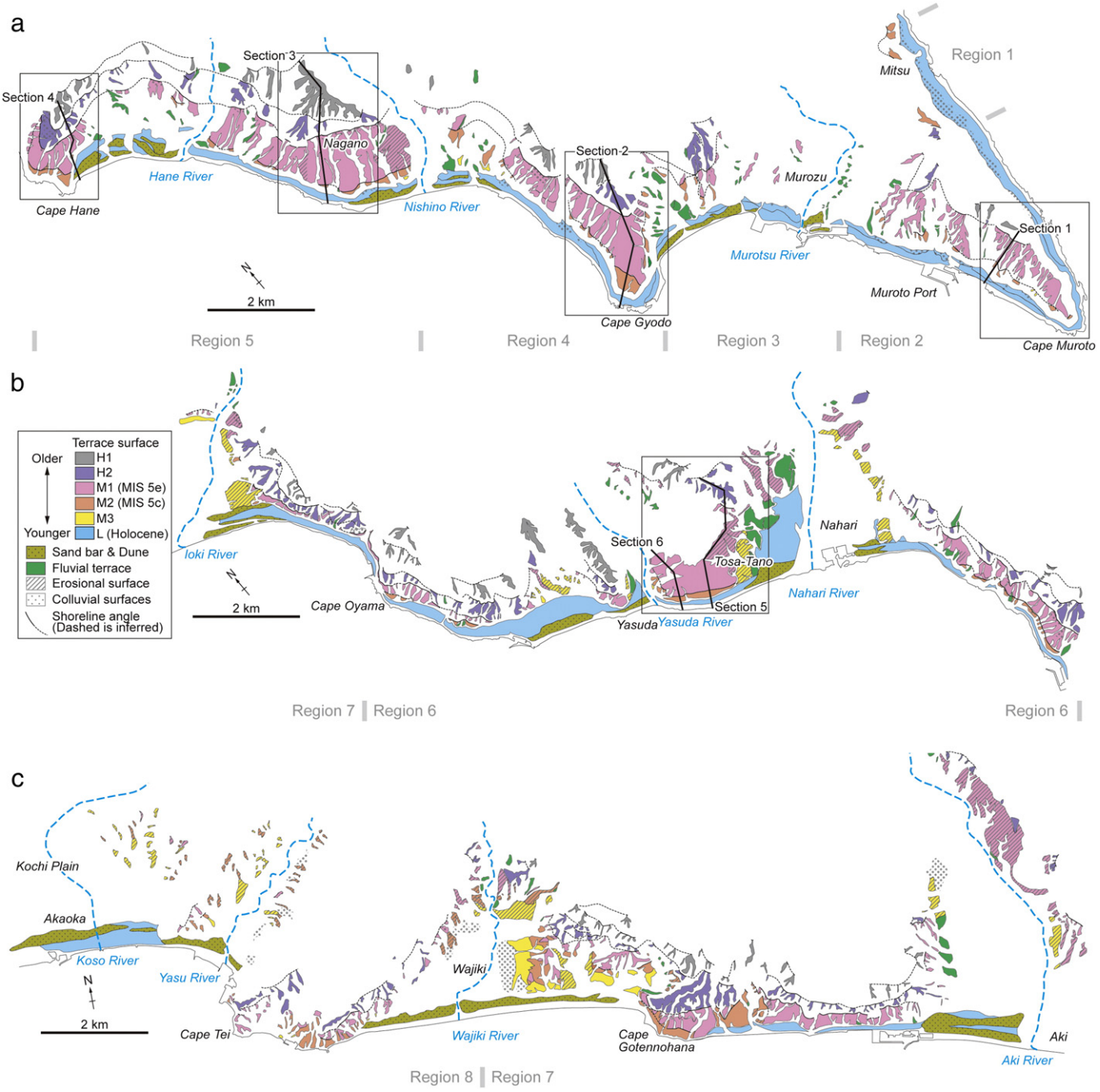

Fig. 3. Maps showing the distribution of marine terraces on the west side of the Muroto Peninsula and locations of geomorphic sections across the terrace inner edges. (a) Regions 1–5. (b) Regions 6 and 7 (southeastern part). (c) Regions 7 (northwestern part) and 8.

paleosols containing the Kikai-Tozurahara (K-Tz) cryptotephra (MIS 5c–5b, ca. 95 ka), are reasonably correlated with MIS 5e (116–132 ka) (Matsu'ura et al., 2011). Consequently, the H1 and H2 terraces are older than MIS 5e, and the M2 and M3 terraces are younger than MIS 5e, but the numerical ages of these terraces are uncertain.

The M1 terrace is widely distributed over the study area. Its inner edge reaches 186 m a.s.l. at Cape Muroto, and it decreases in elevation northwestward to 45–60 m a.s.l. at Cape Tei (Yoshikawa et al., 1964). This trend is interrupted at Cape Gyodo, where the terrace rises to 190 m a.s.l., owing to vertical deformation of the Gyodo-Zaki fault (Research Group for Active Faults of Japan, 1991). The inner edges of the H1, H2, M2, and M3 terraces show a similar deformation. The lower (L) terraces are considered to be of Holocene age (Kanaya, 1978; Maemoku, 1988).

3. Methods

3.1. Marine terrace mapping

Marine terrace levels in the study area were classified by interpretation of 1:10,000 and 1:20,000 scale aerial photographs and by distinguishing and mapping the terrace surfaces on 1:25,000 scale topographic maps. Profiles of each terrace surface constructed from 2-m grid and 10-m grid digital elevation models (DEMs) provided by the Geospatial Information Authority of Japan, were used to determine the elevations of the inner edges of the terrace surfaces. Because 2-m grid DEMs are available only along the coast, most elevations are from the 10-m grid DEM. The 10-m grid DEM was constructed from 1:25,000 scale topographic maps with contour intervals of 5–10 m. Therefore, the error margin of the elevation data is ±5 m.

3.2. Marine terrace dating

The ages of the paleo-sea level indicators were estimated by using tephrostratigraphy (Lowe, 2011). For tephra identification, previously reported tephras shown on isopach maps (Machida and Arai, 2003) extending over the study area were sampled, and the fine sediments or paleosols (which contain cryptotephras) underlying the terrace surfaces were also sampled by coring (rotary cores [66 mm diameter] on the M2 and M1 terraces) or field surveys. Each sample was sieved under running water through disposable 0.125 and 0.0625-mm sieves to prevent contamination from other samples. The residues were dried, embedded in resin, and mounted on slides for determination of grain compositions using a polarizing microscope with point counters, counting 3000 grains per sample.

Cryptotephras were distinguished by examining samples with high concentrations (spikes) of amphibole or quartz. Orthopyroxene was not used because the mineral displays oscillatory zoning and greater compositional variation than amphibole (e.g., Cronin et al., 1996). About 10 quartz and amphibole grains were picked from each of the selected samples and their major-element compositions were analyzed by an electron probe microanalysis (EPMA) system (energy-dispersive spectrometry: Horiba EMAX Energy EX-250) at Furusawa Geological Survey. Nine major elements were measured with a counting time of 150 s, an accelerating voltage of 15 kV, a beam strength of 0.3 nA, and a beam diameter of 150 nm. A 4-μm grid of the targeted glass inclusion within quartz and amphibole grains was scanned. The ZAF procedure was applied to correct for the atomic number effect. The contents of all elements are expressed as weight percentages. The major chemical composition of the amphibole determined by EPMA is expressed as numbers of cations per unit cell (c/uc) on the basis of O (oxygen) = 23 (Table 1).

3.3. Determination of uplift rate and fault slip rate

Rates of uplift were calculated from the elevation differences between the dated sea-level indicators and late Quaternary eustatic sea levels (Stirling et al., 1998; Siddall et al., 2006). Inner-edge elevations of the marine terrace surfaces are useful indicators for mapping the distribution of uplift. Therefore, to estimate accurate uplift rates, high-resolution topographic profiles across terrace inner edges were constructed by using a GPS total station (error margin of 4 cm) in the Nagano (Fig. 4c, Section 3′) and the Tosa-Tano (Fig. 4e, Section 5′) areas. Then, to detect buried sea-level indicators beneath terrace

Table 1
Chemistry of amphibole in tephras from southwestern Japan. The magnesium number, Mg#, is Mg/(Mg + Fe) × 100. FeO* refers to total iron.

	Aso-4 Tosu-Orange flow			Aso-4 Yame flow		Aso-4 ash			Kj-P1		AT	
	Average (n = 9)	SD	Accessory? (n = 1)	Average (n = 10)	SD	Average (n = 9)	SD	Accessory? (n = 1)	Average (n = 10)	SD	Average (n = 10)	SD
SiO_2	43.65	0.28	44.41	43.13	0.61	42.50	0.61	44.27	48.09	0.49	47.08	1.78
TiO_2	3.14	0.12	1.99	3.08	0.36	2.98	0.41	1.96	1.18	0.14	1.22	0.39
Al_2O_3	9.32	0.13	10.08	9.71	0.86	10.96	1.17	9.92	6.57	0.33	6.93	1.65
FeO*	11.07	0.23	13.28	11.04	0.18	10.65	0.97	13.63	12.06	0.28	14.54	0.87
MnO	0.60	0.11	0.46	0.55	0.14	0.34	0.12	0.47	0.66	0.07	0.50	0.13
MgO	14.76	0.13	13.96	14.63	0.22	14.75	0.46	13.60	15.66	0.30	14.06	1.09
CaO	11.07	0.14	11.28	11.10	0.14	11.37	0.26	11.30	10.86	0.13	10.46	0.34
Na_2O	2.28	0.08	1.77	2.25	0.09	2.41	0.06	1.70	1.15	0.06	1.15	0.25
K_2O	0.76	0.05	0.51	0.68	0.16	0.61	0.08	0.54	0.34	0.05	0.29	0.05
Cr_2O_3	0	0	0	0	0	0	0	0	0	0	0	0
Total	96.64	0.41	97.74	96.17	0.83	96.57	0.84	97.39	96.57	0.71	96.22	0.8
Cations per unit cell on the basis of O = 23.00												
Si	6.48	0.02	6.54	6.44	0.07	6.31	0.09	6.56	7.07	0.05	7.02	0.24
Al	1.63	0.02	1.75	1.71	0.15	1.92	0.19	1.73	1.14	0.06	1.22	0.30
Ti	0.35	0.01	0.22	0.35	0.04	0.33	0.05	0.22	0.13	0.02	0.14	0.04
Fe	1.38	0.03	1.64	1.38	0.03	1.32	0.13	1.69	1.48	0.03	1.81	0.12
Mn	0.07	0.01	0.06	0.07	0.02	0.04	0.01	0.06	0.08	0.01	0.06	0.02
Mg	3.27	0.02	3.07	3.25	0.04	3.26	0.07	3.00	3.43	0.06	3.12	0.23
Ca	1.76	0.02	1.78	1.78	0.02	1.81	0.03	1.79	1.71	0.02	1.67	0.05
Na	0.66	0.02	0.51	0.65	0.02	0.69	0.02	0.49	0.33	0.02	0.33	0.08
K	0.14	0.01	0.10	0.13	0.03	0.12	0.02	0.10	0.06	0.01	0.05	0.01
Cr	0.00	0.00	0.00	0.00	0.00	0.00	0.00	0.00	0.00	0.00	0.00	0.00
Mg#	70.39	0.57	65.20	70.26	0.59	71.17	2.46	64.01	69.83	0.78	63.20	3.29

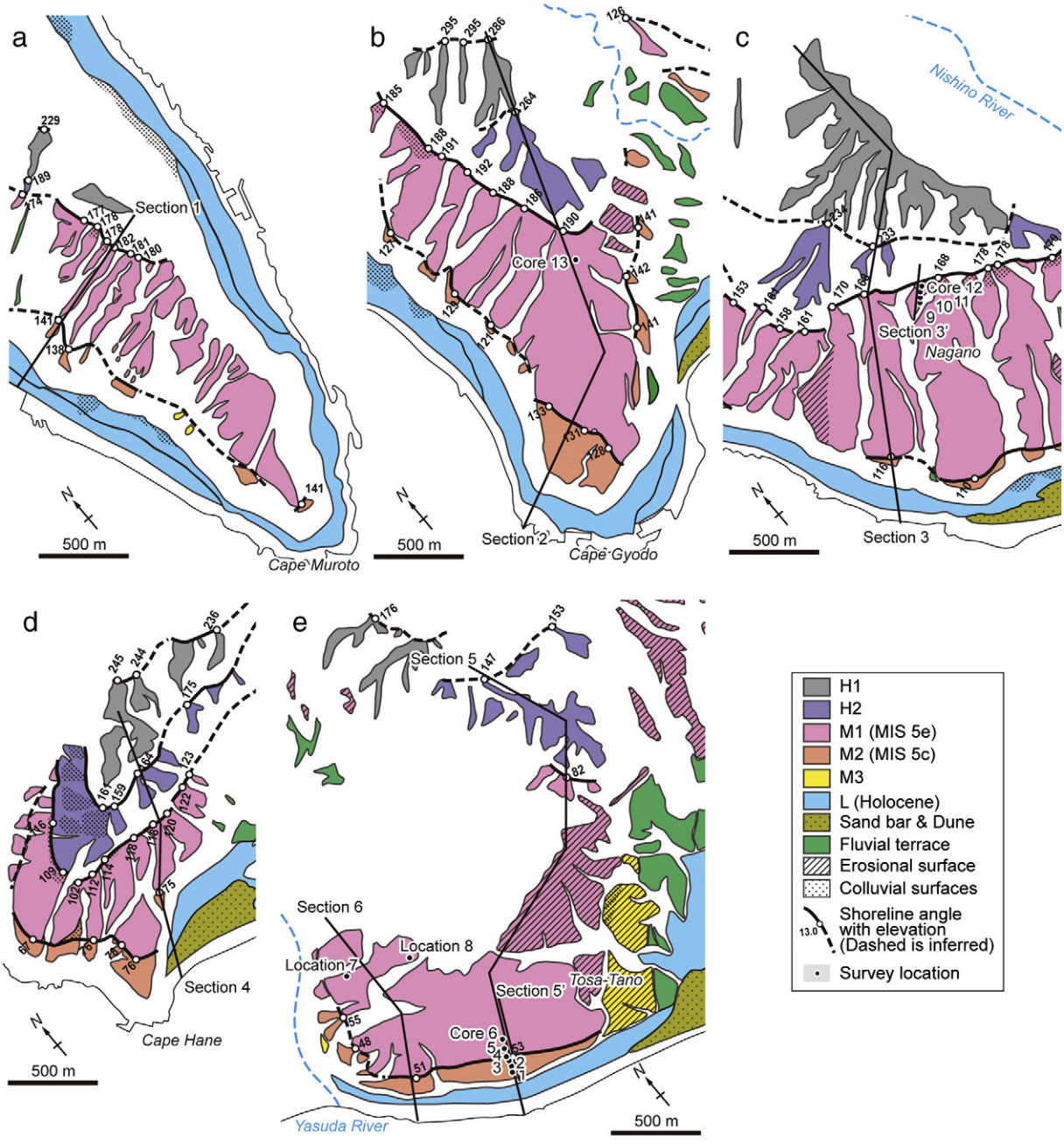

Fig. 4. Detailed terrace maps and locations of topographic cross sections. Locations are shown in Fig. 3.

deposits, rotary cores (66 mm diameter) were obtained along the profiles at four locations in the Nagano area (Fig. 5d) and six locations in the Tosa-Tano area (Fig. 5e). These data yielded the location of the shoreline angle beneath the terrace surface as well as the spatial variation in sediment thickness.

The stratigraphy of the deposits overlying each rock-cut terrace was interpreted by comparison with coastal deposits on the modern wave-cut platform, and buried wave-cut platforms were identified by analogy with the modern coast. The elevation of the buried shoreline angle was estimated after reconstructing the bedrock profiles of the wave-cut platforms and the slopes (paleo-sea cliffs) behind them.

To estimate the shortening and slip rates of offshore faults, terrace deformation (the excess area by fault-related uplift) on the hanging wall was used as the basis of a mass-balance calculation (Chamberlin, 1910; Epard and Groshong, 1993; Bernard et al., 2007).

4. Sequences and ages of tephras and terraces

4.1. Pleistocene tephras

Previously published isopach maps (Machida and Arai, 2003) indicated that several tephras of Pleistocene age were likely to occur in terrace deposits.

4.1.1. Aira-Tn tephra

The Aira-Tn tephra (AT) was erupted from the Aira caldera in southern Kyushu (Fig. 1b; Machida and Arai, 2003). AT is dated at 28.55 ka on the basis of its stratigraphic position in the uppermost part of MIS 3 marine sediments (Aoki, 2008). Its reported mineral assemblage consists of orthopyroxene, clinopyroxene, quartz, and a small amount of amphibole (Kawai and Miyake, 1999; Machida and Arai, 2003; Kawamura, 2009).

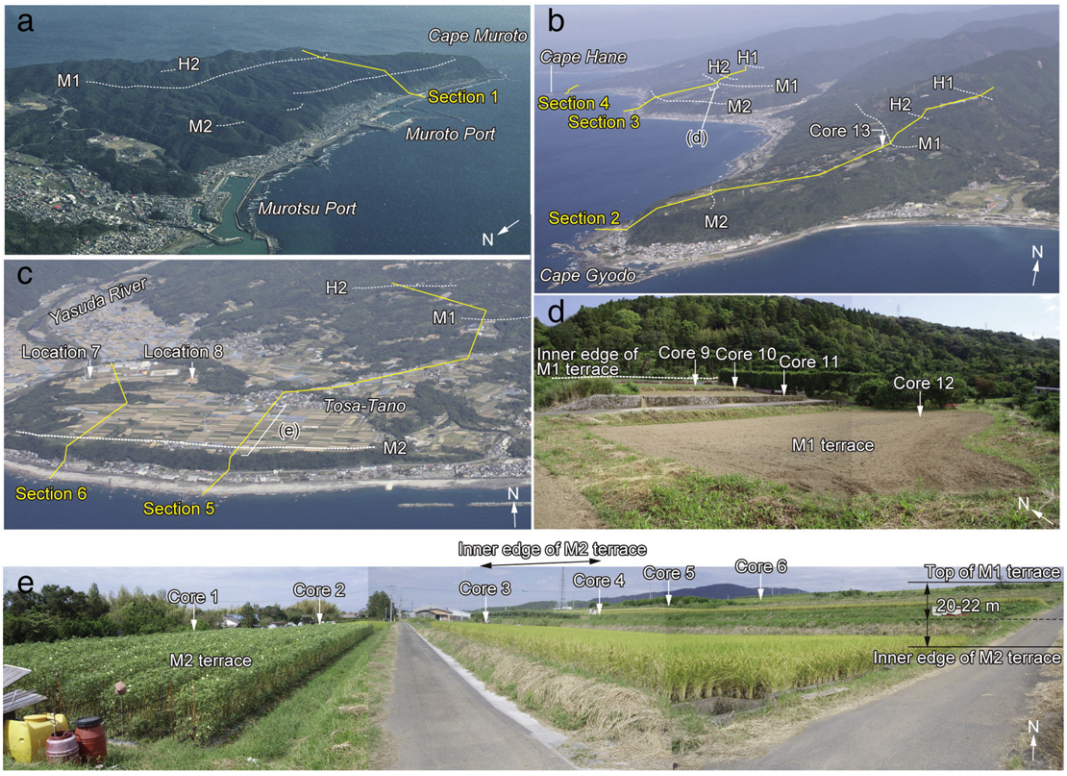

Fig. 5. Photographs of marine terraces (locations shown by dotted lines) on the Muroto Peninsula. (a) Marine terraces near Cape Muroto showing the location of Section 1. Photo provided by the Shikoku Regional Development Bureau, Ministry of Land, Infrastructure, Transport and Tourism. (b) Marine terraces at Cape Gyodo and Cape Hane showing locations of Sections 2, 3, and 4. Photo provided by Kochi Prefecture. (c) Marine terraces in the Tosa-Tano area showing locations of Sections 5 and 6. Photo provided by Kochi Prefecture. (d) Inner edge of the M1 terrace surface and core locations on Section 3′. Photo site shown in (b). (e) Inner edge of the M2 terrace surface and core locations on Section 5′. Photo site shown in (c).

AT was sampled for chemical analysis from airfall deposits in southwestern Shikoku (N32.968257, E132.687833: location 3 of Matsu'ura et al., 2011). Its amphibole chemistry shows that Mg# (the magnesium number, Mg/(Mg + Fe) × 100) of AT is lower than those of tephras Kuju-1 and Aso-4, described below (Table 1).

4.1.2. Kuju-1 tephra

The Kuju-1 tephra (Kj-P1) was erupted from the Kuju caldera in central Kyushu (Fig. 1b; Machida and Arai, 2003). Its reported thickness is 20–40 cm within fluvial terrace deposits in southwestern Shikoku (Kumahara and Nagaoka, 2002), but it has not been reported on the Muroto Peninsula. Its eruptive age is constrained by a radiocarbon age older than 40,000 ^{14}C y BP (Okuno et al., 1998) and a fission-track age of 70–80 ka (Kamata et al., 1998). These ages are consistent with its stratigraphic position between tephras AT and Aso-4. In this study, an age range of 40–80 ka was assigned to Kj-P1.

Kj-P1 was sampled for chemical analysis from pyroclastic flow deposits at the reported outcrop (N33.030954, E131.301638: Kamata and Hoshizumi, 1996). Its amphibole chemistry shows relatively high Si, low Al, low Ti, and low Na contents (Table 1).

4.1.3. Aso-4 tephra

The Aso-4 tephra (Aso-4) was erupted from the Aso caldera in central Kyushu (Fig. 1b; Machida and Arai, 2003). Its eruptive age is 86.8–87.3 ka, derived from its stratigraphic position in MIS 5b marine sediments (Aoki, 2008). Its mineral assemblage consists of orthopyroxene, clinopyroxene, and amphibole (Machida and Arai, 2003). Aso-4 has been identified in terrestrial sediments in northern Shikoku on the basis of refractive indices and orthopyroxene chemistry (Morie et al., 2001; Kawamura, 2009). However, on the Muroto Peninsula, glass shards are absent because of dissolution. Therefore, a resistant mineral such as amphibole, which has not been previously investigated in this tephra, is probably useful for correlation of Aso-4.

Aso-4 was sampled for chemical analysis from several deposits in Kyushu: Tosu-Orange pyroclastic flow deposits (Furusawa, 2003: N33.255852, E131.308833), Yame pyroclastic flow deposits (Ono, 1996: N33.063333, E131.384166), and airfall deposits in central Japan (Kimura, 1996: N36.545326, E138.039833). The amphiboles in these samples are similar, with high Al, Ti, Na, and K contents (Table 1). Aso-4 has not been reported in sediments on the Muroto Peninsula.

4.1.4. Kikai-Tozurahara tephra

The Kikai-Tozurahara tephra (K-Tz) was erupted from the Kikai caldera off the coast of southern Kyushu (Fig. 1b; Machida and Arai, 2003). Its eruptive age is MIS 5c–5b from its stratigraphic position between the Ontake-Pumice 1 (MIS 5c) and Aso-4 tephras (MIS 5b: Machida and Arai, 2003). Its mineral assemblage consists of orthopyroxene, clinopyroxene, and quartz (Machida and Arai, 2003). Quartz of K-Tz is characterized by euhedral high-quartz grains (Machida and Arai, 2003), and its quartz grains have occasional melt inclusions (Furusawa and Nakamura, 2009).

Matsu'ura et al. (2011) assigned quartz grains found in fine sediments of a paleosol in the terrace deposits at location 7 in the Tosa-Tano area (Figs. 4e and 5c) to K-Tz on the basis of their glass inclusion chemistry (high SiO_2 content, 78.85 wt.%; Table 2). However, glass shards and pyroxene grains of this tephra in these sediments have been dissolved by weathering.

4.2. Sequences and ages of terraces

4.2.1. L and M3 terraces

The L terrace surfaces occur along the modern coast of Cape Muroto (Fig. 3). These terraces are divided into a higher and a lower group and are considered to be of Holocene age. On Cape Muroto they are considered to be emergent terraces associated with large earthquakes caused by offshore faults (Maemoku, 1988, 2001). Radiocarbon dates on sessile

Table 2
Major-element compositions of melt inclusions in high-quartz grains (normalized). Melt inclusion data of sample 708 (tephra K-Tz) are those of samples 2–8 in Matsu'ura et al. (2011). Sampling horizons are shown in Fig. 7. FeO* refers to total iron.

	Sample 101										Sample 708 (K-Tz)	
	1	2	3	4	5	6	7	8	Average ($n = 8$)	SD	Average ($n = 13$)	SD
SiO_2	78.94	79.10	78.92	79.30	78.47	79.13	78.55	79.25	78.96	0.29	78.85	0.25
TiO_2	0.18	0.14	0.28	0.16	0.50	0.31	0.31	0.28	0.27	0.11	0.25	0.09
Al_2O_3	11.45	11.35	11.41	11.29	11.53	11.24	11.63	11.46	11.42	0.12	11.68	0.23
FeO*	1.12	1.10	1.03	1.02	1.09	1.03	1.16	0.93	1.06	0.07	1.07	0.12
MnO	0.04	0.00	0.10	0.10	0.02	0.00	0.05	0.03	0.04	0.04	0.05	0.06
MgO	0.19	0.22	0.12	0.16	0.18	0.24	0.17	0.15	0.18	0.04	0.18	0.04
CaO	1.15	1.07	1.09	1.08	1.27	1.08	1.19	1.00	1.11	0.08	1.08	0.11
Na_2O	3.34	3.47	3.44	3.46	3.46	3.46	3.42	3.36	3.42	0.05	3.32	0.30
K_2O	3.59	3.56	3.62	3.43	3.48	3.51	3.52	3.54	3.53	0.05	3.52	0.16
Total	100.00	100.00	100.00	100.00	100.00	100.00	100.00	100.00	100.00		100.00	
Diameter of glass inclusion (μm)	17	15	11	11	11	10	10	9				

organisms indicate that the two latest large earthquake events were at ca. 1.0 and 2.8 ka.

The M3 terrace surface occurs only locally near the mouths of rivers, such as the Nahari, Ioki, and Wajiki Rivers (Fig. 3). At some places along these rivers, the terrace surface has probably been eroded to form a lower terrace surface. Yoshikawa et al. (1964) reported that the M3 terrace formed as a fluvial terrace because the terrace deposits consist of unsorted subangular gravel clasts such

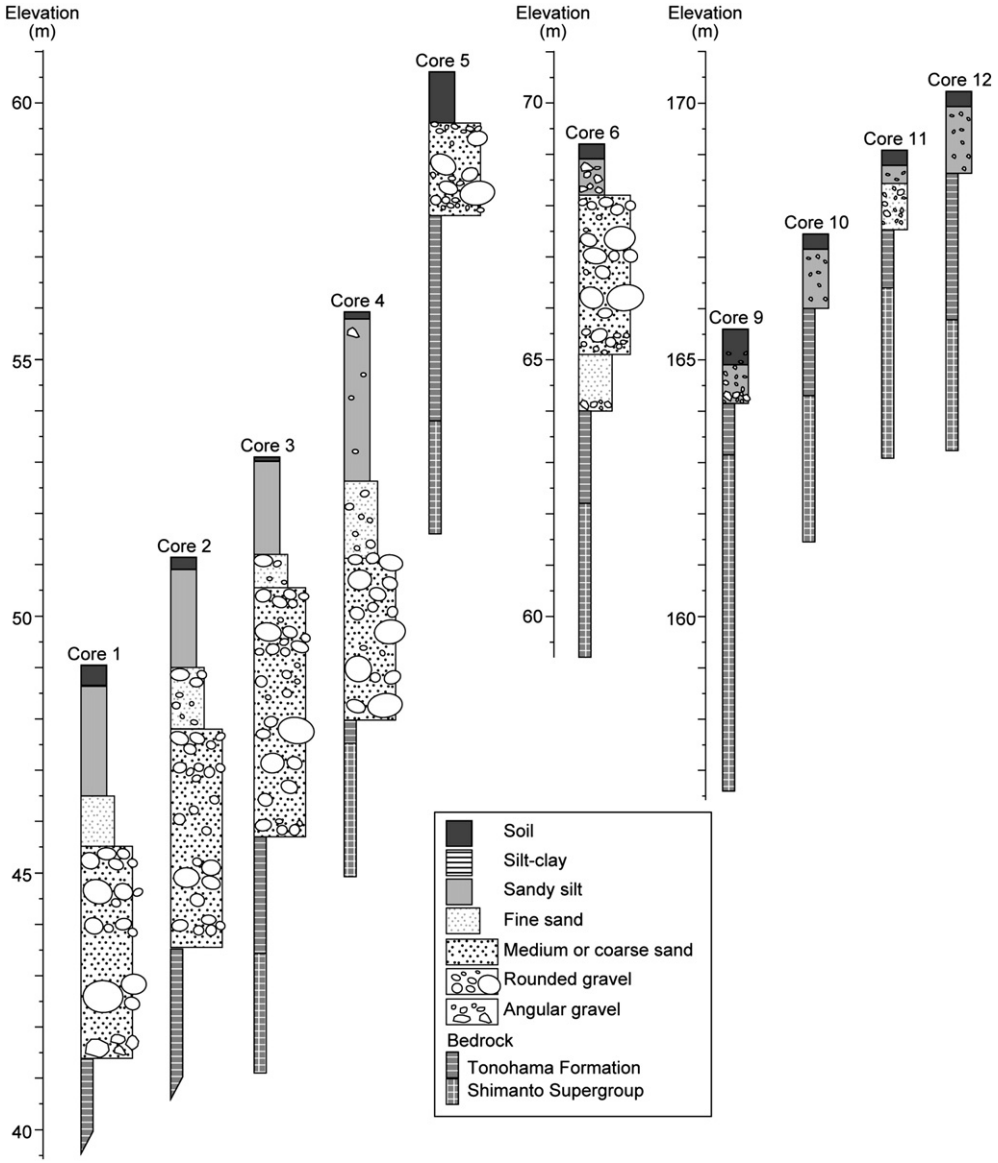

Fig. 6. Geologic columns of drill cores. Locations of drill sites are shown in Fig. 4. Cores 1 to 6 are from the Tosa-Tano area; cores 9 to 12 are from the Nagano area.

as those observed in the modern riverbed. The M3 terrace surface has no age indicator.

4.2.2. M2 terrace

The M2 terrace surface is landward with respect to the L terrace surfaces (Fig. 3). M2 terrace deposits were found only in drill cores, not outcrops.

In cores 1–4 from this terrace along Section 5 (Figs. 4e, 5e), the sediments consist, in ascending order, of bedrock (Shimanto Supergroup and Tonohama Formation), gravel with sand, sand with gravel, sandy silt, and soil (Fig. 6). The gravel-bearing beds are 4.7–5.5 m thick and slightly thinner toward the terrace inner edge (core 4). Above these sediments, massive deposits of brownish sandy silt with minor amounts of granules are 1.8–3.2 m thick, thicker toward the terrace inner edge. These finer sediments correspond to a paleosol, and the granules are colluvium from the adjoining slope.

No tephra was visible in any M2 terrace deposits. However, the paleosol in the M1 terrace deposits included some cryptotephras

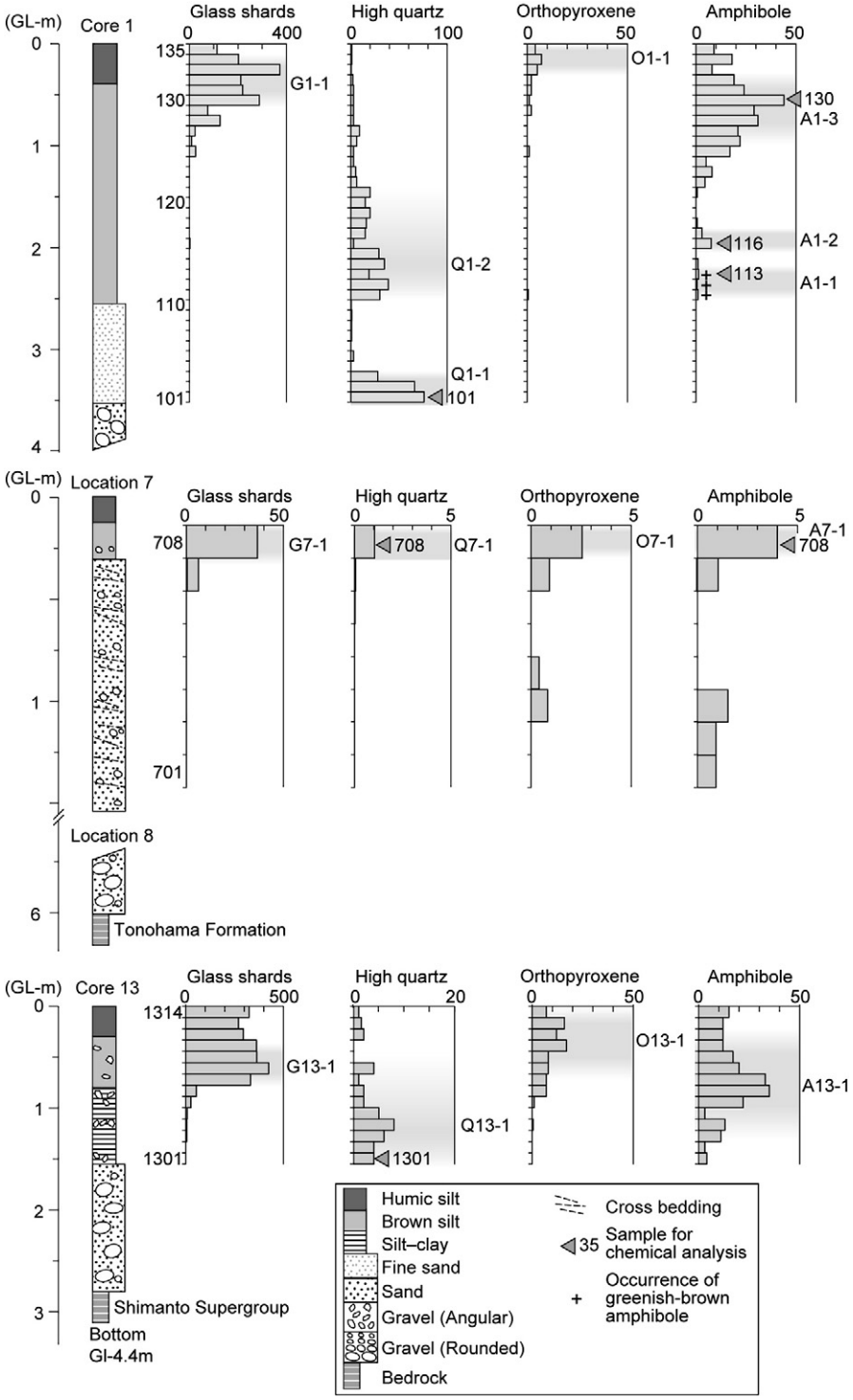

Fig. 7. Geologic columns of the outcrop at location 7 and drill cores 1 and 13 showing the distributions of tephra grains in the sediments. The histograms show the numbers of glass shards and grains of high quartz, orthopyroxene, and amphibole per 3000 tephra grains. GL, ground level.

at location 7 (Matsu'ura et al., 2011). Therefore, to search for cryptotephras, the fine deposits of the uppermost M2 terrace deposits and paleosol were targeted, and the fine sediments in core 1 in particular were sampled (Fig. 7) because they were relatively free of gravel.

Glass shards were abundant in horizon G1-1 (samples 130–134) and scarce below it (Fig. 7). High-quartz grains were abundant in horizons Q1-1 and Q1-2 (samples 101–103 and 111–115, respectively) and gradually decreased upward. Orthopyroxene grains were found in small amounts in horizon O1-1 (samples 133-135). Amphibole grains were abundant in horizons A1-2 and A1-3 (samples 116–117 and 125–132, respectively), and those in horizon A1-1 (samples 111–113) had a characteristic brownish green color, distinct from the green grains in other horizons.

To refine the cryptotephra stratigraphy and terrace chronology, sample 101 from horizon Q1-1, where the concentration of high-quartz grains was highest, and samples 113, 116, and 130 from horizons A1-1, A1-2, and A1-3, respectively, were selected for chemical analyses.

The melt inclusions in high-quartz grains from sample 101 had a high SiO_2 content (78.47–79.30 wt.%, Table 2; Fig. 8) and were generally similar in chemical composition to the reported data from tephra K-Tz at location 7 on the M1 terrace surface (Matsu'ura et al., 2011). The targeted melt inclusions, which were 9–17 μm in diameter (much larger than the 4-μm EPMA grid), were appropriate for major-element analysis.

The analysis results of amphibole grains from samples 113, 116, and 130 are compared with the K-Tz tephra (sample 708) and other tephras in Fig. 9. The composition of sample 113 overlaps the tephra Aso-4 population. The compositions of samples 116 and 130 are consistent with the Kj-P1 population but not with the AT population, therefore either sample 116 or sample 130 is correlated to Kj-P1. Sample 130, from horizon A1-3, may include grains transferred by bioturbation from a lower horizon (A1-2), from which sample 116 was obtained. However, horizon A1-3 contains a large number of amphibole grains and is therefore likely correlated with Kj-P1, which in southwestern Shikoku includes abundant amphibole grains (Kumahara and Nagaoka, 2002). Horizon A1-2 has few amphibole grains and does not correspond to any tephra layer from Kuju or its neighboring volcanoes.

In summary, horizons Q1-1, A1-1, A1-2, and A1-3, in ascending order, are reasonably correlated with K-Tz, Aso-4, an unnamed tephra, and Kj-P1, respectively. The occurrences of tephra K-Tz in the uppermost M2 terrace deposits and tephra Aso-4 at the bottom of the paleosol suggest that the M2 terrace dates to MIS 5c (Fig. 10).

4.2.3. M1 terrace

The M1 terrace surface is landward with respect to the M2 terrace. The surface is well preserved along the present coast (Fig. 3) but along some rivers a lower surface has been cut in M1 by erosion. M1 terrace deposits were observed at locations 7 and 8 (Figs. 4e; 5c) and in core 13 (Figs. 4b; 5b). Terrace deposits at location 8, which unconformably overlie the Tonohama Formation, are about 6 m thick and consist of clasts ranging in size from sand to boulders (Maemoku, 1996; Matsu'ura et al., 2011) (Fig. 7). Terrace deposits at location 7 are over 1.5 m thick and consist of cross-laminated sand with granules (Matsu'ura et al., 2011). Massive deposits of brownish silt to fine sand with a few granules (0.2 m thick) and humic silt, corresponding to a paleosol and cultivated soil, respectively, overlie the terrace deposits at location 7. The paleosol includes horizons containing abundant glass shards (G7-1), high quartz (Q7-1), orthopyroxene (O7-1), and

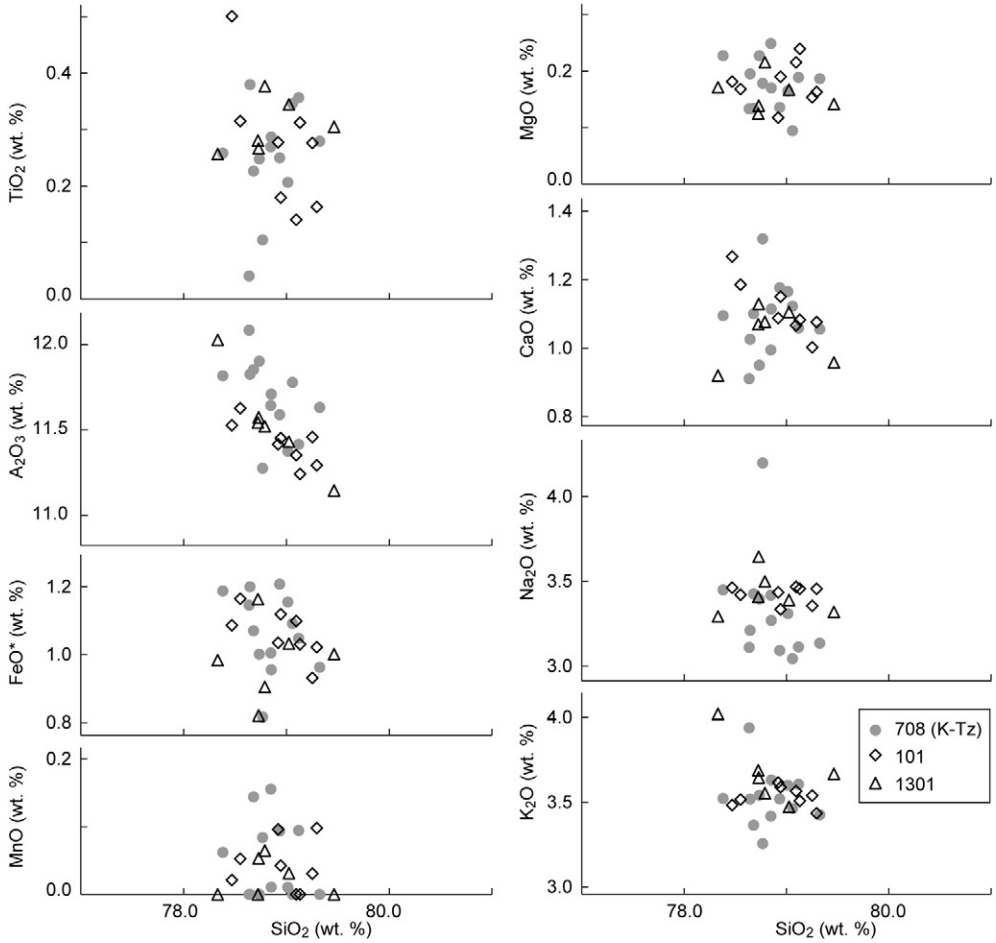

Fig. 8. Glass (melt) inclusion chemistry of high-quartz grains. High quartz in sample 708 has been correlated with tephra K-Tz.

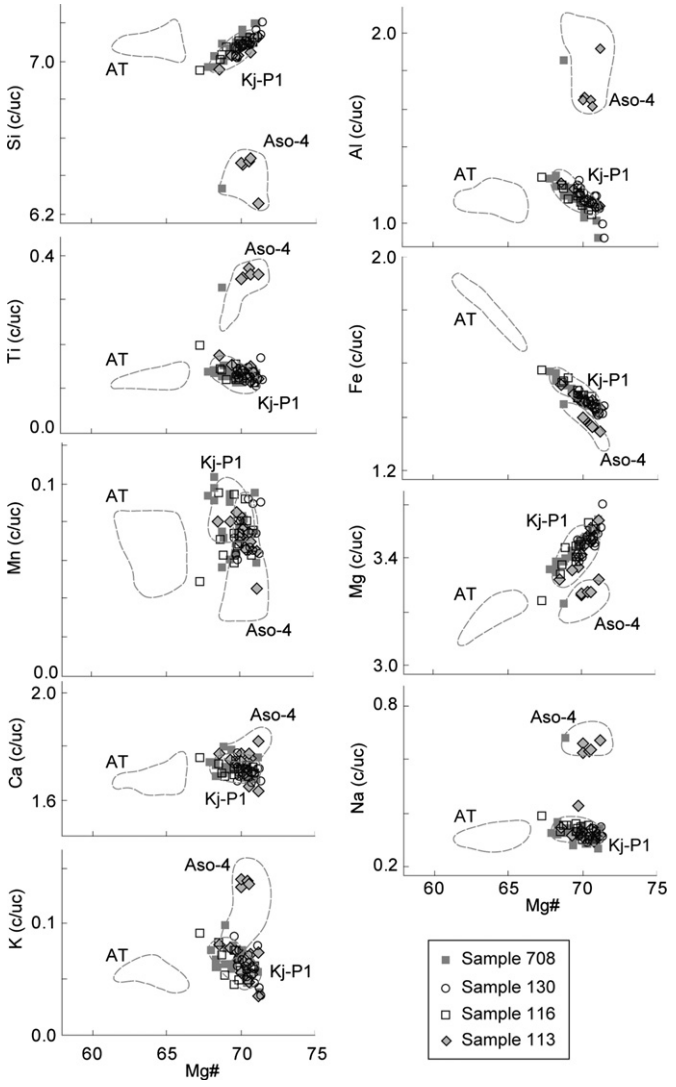

Fig. 9. Amphibole chemistry of tephra samples. The *y* axis shows cations per unit cell (c/uc). The magnesium number, Mg#, is Mg/(Mg + Fe) × 100.

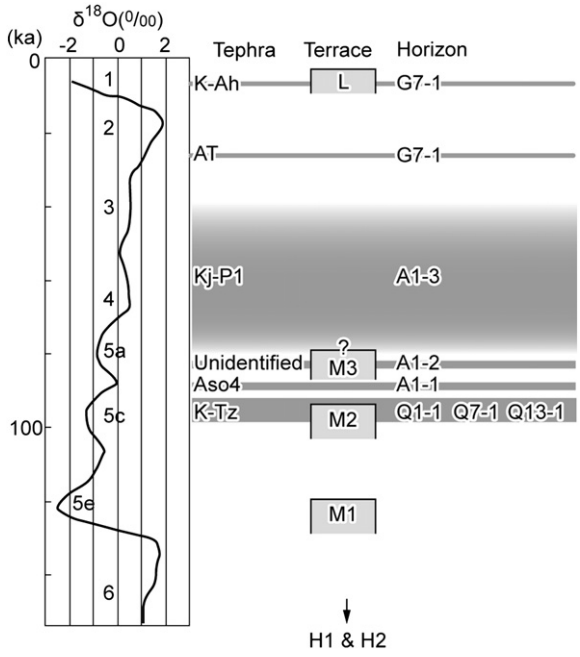

Fig. 10. Stratigraphic relations between tephras and terraces. The $\delta^{18}O$ curve is from Bassinot et al. (1994).

amphibole (A7-1) (Fig. 7). In core 13, the terrace deposits, which are 1.25 m thick and consist of boulders, unconformably overlie the Shimanto Supergroup. The overlying silt with angular gravel (0.75 m thick), massive deposits of brownish silt to fine sand with minor granules (0.5 m thick), and humic soil correspond to colluvium, a paleosol, and cultivated soil, respectively.

On the basis of analyses of melt inclusions in high-quartz grains, Matsu'ura et al. (2011) correlated the quartz grains of horizon Q7-1 (sample 708) with tephra K-Tz because of their high SiO_2 content (78.75 ± 0.25 wt.%, Table 2; Fig. 8). Compositions of amphiboles from horizon A7-1 (sample 708) overlap those of tephra Kj-P1, but one data point of a single amphibole grain matches the tephra Aso-4 population (Fig. 9). It is likely that both these tephras occur within the paleosol because the sedimentation rate of the parent material of the paleosol appears to have been very slow. Glass shard data show that horizon G7-1 includes the Aira-Tn and Kikai-Akahoya cryptotephras (Matsu'ura et al., 2011). Because the inferred age of the M2 terrace deposits is MIS 5c, as described in Section 4.2.2, the M1 terrace deposits can be confidently correlated with a sea-level highstand, probably during MIS 5e (Fig. 10).

4.2.4. H2 and H1 terraces

The H2 terrace surface is landward with respect to M1. The surface is dissected, but its inner edge is clear. Given the assignment of the M1 terrace deposits to MIS 5e, the H2 terrace deposits must correspond to an earlier highstand, probably MIS 7.

The group of H1 terrace surfaces is landward of H2, and they may include some surfaces older than H2 (Fig. 3). The terraces are highly dissected, and their inner edges are not clear.

5. Uplift rate distribution inferred from the marine terrace surfaces

5.1. Elevations of the inner edges of terrace surfaces

Selected longitudinal profiles of terrace surfaces constructed from the DEMs are shown in Fig. 11. The M1 terrace inner edge is prominent in these profiles and widely preserved, as shown by its occurrence in Sections 1–5. The M1 terrace surface often includes steps, or subsidiary inner edges (e.g., Section 2, Fig. 11b), but whether these steps record paleo-sea levels during MIS 5e is uncertain. The inner edge of the M2 terrace in these profiles is sometimes unclear; for example, in Section 3 (Fig. 11c), the preserved surface is too narrow to be discriminated from the slope behind it. However, the M2 inner edge often provides paleo-sea level information where the M1 terrace inner edge cannot be identified (e.g., Sections 5 and 6; Fig. 11e, f). The H2 terrace inner edge is higher than the M1 terrace inner edge, indicating continuous uplift during the late Quaternary (Sections 2–5). However, the H1 terrace inner edge is not well preserved even where the terrace surface is evident.

The elevations of terrace inner edges obtained from the constructed longitudinal (i.e., from offshore to onshore) profiles (Fig. 4) were plotted on a section extending along the western side of the Muroto Peninsula from Cape Muroto to the Kochi Plain (Fig. 12). This profile was then divided from east to west into eight tectonic regions on the basis of the terrace inner edge elevation data as described below (Table 3).

Region 1: The M2 inner edge (MIS 5c) is at 117–132 m a.s.l., and its elevation decreases eastward, consistent with its position on the forelimb of the Muroto–Misaki anticline.

Region 2: The M1 and M2 terrace inner edges reach 182 and 141 m a.s.l., respectively, on the axis of the Muroto–Misaki anticline. This decrease westward in the region to 164 m a.s.l. (M1) and 119 m a.s.l. (M2), is consistent with the backlimb deformation of the anticline inferred from marine geologic data (Okamura, 1990).

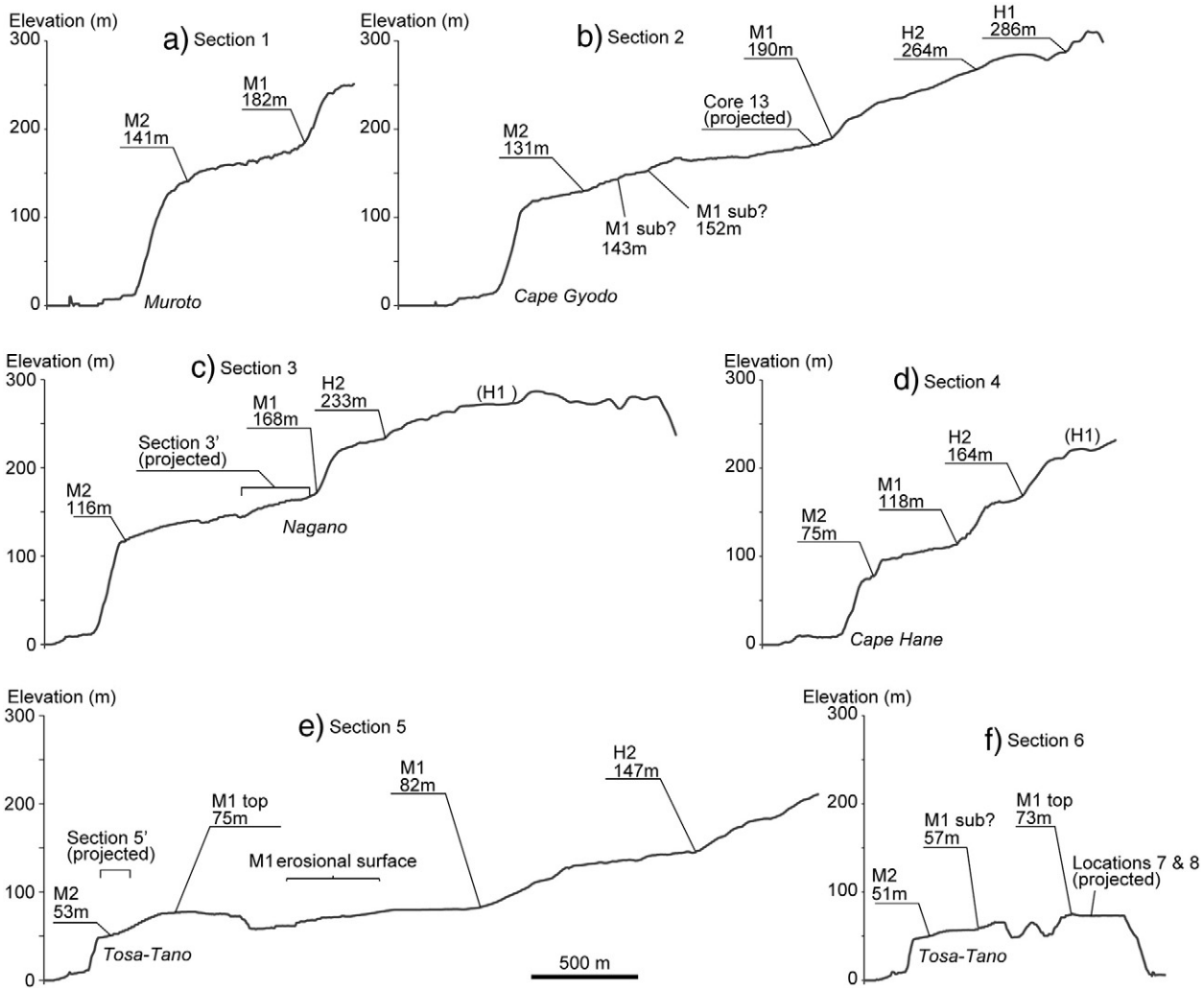

Fig. 11. Profiles of marine terrace surfaces along Tosa Bay. Locations of sections are shown in Fig. 4.

Region 3: The M1 and M2 terrace inner edges are at 126–143 and 109–119 m a.s.l., respectively, apparently lower than in regions 2 and 4.

Region 4: The terrace inner edges abruptly increase to 192 m a.s.l. (M1) and 142 m a.s.l. (M2) at the eastern end of the region. This elevation change between regions 3 and 4 (about 70 m for M1 and 50 m for M2) is probably due to vertical deformation by the Gyodo-Zaki fault. The terrace inner edges decrease westward to 165 m a.s.l. (M1) and 119 m a.s.l. (M2), indicating westward tilting.

Region 5: The M1 inner edge is at 178 m a.s.l. at the eastern end of the region and is offset upward by about 15 m with respect to the western edge of region 4, probably as a result of vertical deformation by the Kiragawa fault. However, the M2 inner edge does not show this vertical

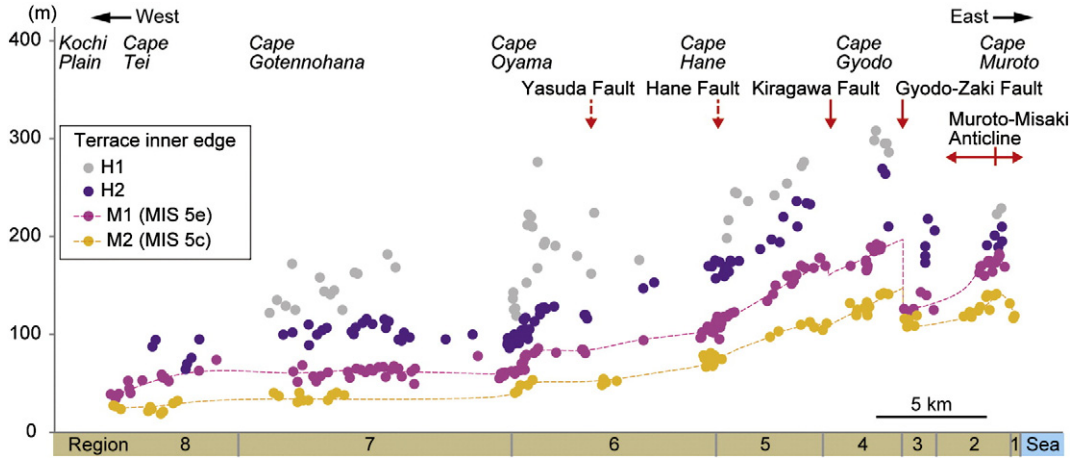

Fig. 12. Profiles of marine terrace surfaces along the west side of the Muroto Peninsula (locations in Fig. 2). Locations of active faults are also shown.

Table 3
Elevations of terrace inner edges and inferred uplift rates for regions 1–8 (locations in Fig. 3).

Region	H1 (MIS 7 or 9?) & H2 (MIS 7)		M1 (MIS 5e)		M2 (MIS 5c)	
	Elevation (m)	Uplift rate (m ky^{-1})	Elevation (m)	Uplift rate (m ky^{-1})	Elevation (m)	Uplift rate (m ky^{-1})
1 Mitsu					117–132	1.3–1.5
2 Muroto–Murozu River	189–229	0.8–1.3	164–182	1.2–1.6	119–141	1.3–1.6
3 Murozu River–Cape Gyodo	190–218	0.8–1.2	126–143	0.9–1.2	109–119	1.2–1.4
4 Cape Gyodo–Nishino River	264–308	1.1–1.5	165–192	1.2–1.7	119–142	1.3–1.6
5 Nishino River–Cape Hane	159–276	0.7–1.5	102–178	0.7–1.5	67–113	0.8–1.3
6 Cape Hane–Cape Oyama	91–276	0.4–1.5	60–118	0.4–1.0	40–81	0.5–1.0
7 Cape Oyama–Wajiki River	86–182	0.4–1.0	49–78	0.3–0.7	31–41	0.4–0.5
8 Wajiki River–Koso River	64–95	0.3–0.6	34–74	0.2–0.6	19–32	0.3–0.4

offset. The terrace inner edges decrease westward to 102 m a.s.l. (M1) and 67 m a.s.l. (M2), indicating westward tilting.

Region 6: The elevations of the terrace inner edges decrease to 60–70 m (M1) and 40–50 m a.s.l. (M2) at the western end, more gradually than in region 5. There is no clear offset across the traces of the Hane and Yasuda faults. There is an abrupt change, however, at the boundary between regions 6 and 7, although no active fault has been reported there. Instead, this change is interpreted to indicate an axial surface (kink), marking the edge of the backlimb of the anticline and caused by a bend in the subsurface fault (Suppe, 1983; also described in Section 7.1).

Region 7: The elevations of the M1 and M2 inner edges are approximately constant in this region.

Region 8: The elevations of the M1 and M2 terrace inner edges decrease westward to a minimum of 34 and 19 m a.s.l., respectively.

This profile of uplift along the Muroto Peninsula is similar to that described by Yoshikawa et al. (1964), but it includes new data for region 1.

The inner edge elevations of the H2 terrace surface lie above those of terraces M1 and M2. Although H2 may comprise two or three terraces, corresponding to substages of MIS 7, its deformation pattern closely follows those of the M1 and M2 terrace inner edges. Likewise, the H1 terraces show crustal deformation roughly similar to that of the younger terrace surfaces.

5.2. Uplift rates inferred from the inner edge elevations of terrace surfaces

As described in Sections 4.2.2 and 4.2.3, the correlations of the M2 and M1 terraces with MIS 5c and MIS 5e, respectively, were based on stratigraphic information from paleosols and marine terrace deposits. Uplift rates of these terrace surfaces were calculated by using an age of 94–100 ka for MIS 5c (Bassinot et al., 1994) and a eustatic sea level of about −10 m relative to the present (Stirling et al., 1998) (M2), and an age of 113–132 ka for MIS 5e and a eustatic sea level of 0 to 6 m relative to the present (Siddall et al., 2006) (M1). During MIS 7, the probable age of the H2 terrace (see Section 4.2.4), sea level peaked three times, but the H2 terrace could not be correlated with any particular substage. To calculate uplift of the H2 terrace, ages of 230–235, 212–220, and 190–201 ka were used for MIS 7e, 7c, and 7a, respectively. A eustatic sea level of −5 to −15 m was used for all three substages (Siddall et al., 2006), although the sea level estimates include considerable uncertainties. The position of the H1 terrace in MIS chronology could not be determined, but for the purpose of the uplift calculation it was assumed to correlate with MIS 7.

The calculated uplift rates in regions 1–8 are listed in Table 3. Within each region, the M1 and M2 terrace uplift rates inferred from their inner edge elevations are similar. Together, these rates indicate an anticlinal deformation: high uplift rate (1.3–1.5 m ky^{-1}) on the forelimb (region 1), high uplift rate (1.2–1.6 m ky^{-1}) on the anticlinal axis (region 2), and westward tilting on the backlimb (regions 3–6). The uplift rate in region 4 (1.2–1.7 m ky^{-1}) is higher than the rates in other regions because of vertical deformation by the Gyodo-Zaki fault. The rates decrease northwestward to 0.3–0.7 m ky^{-1} in region 7 and 0.2–0.6 m ky^{-1} in region 8. The rates in region 7 are roughly constant and likely represent the regional uplift rate for the Muroto Peninsula. Because data are not available for the western side of region 8, it could not be determined whether uplift in that region is local or regional. Uplift rates inferred from terraces H1 and H2, despite their large error margins, are also consistent with those inferred from terraces M1 and M2.

6. Uplift rates inferred from buried shoreline angles

6.1. Buried shoreline angle beneath terrace M2

The elevation of the inner edge of the M2 terrace surface is about 54–55 m in Section 5′, which is at the southern end of Section 5 (Figs. 4e; 13a). The M2 terrace deposits do not contain biological sea-level indicators in the form of fossils. Therefore, the sedimentary sequence of the terrace deposits was interpreted by analogy with the modern coastal stratigraphy. At the inner edge of the M2 terrace surface, the cores document a succession in ascending order of bedrock, gravel, sand with gravel, sandy silt (paleosol), and modern soil (Fig. 6).

Similarly, on the modern Tosa-Tano coast, the bedrock is often overlain by several meters of rounded gravel. Because the gravel beds on both the modern and old (relict) rock-cut surfaces are very similar in thickness and clast roundness, the rounded gravel in the M2 terrace deposits was interpreted as paleo-coastal deposits and the bedrock strath surface of the M2 terrace as a wave-cut platform. These features date from MIS 5c because the deposits include tephra K-Tz (MIS 5c–5b) and are overlain by a paleosol that includes tephras Aso-4 (MIS 5b) and Kj-P1 (40–80 ka) (Fig. 10).

The inner edge of the M2 terrace surface in Section 5′ has been degraded as a geomorphic sea-level indicator by artificial modification, but it sits at roughly 54–55 m a.s.l. between the sites of cores 3 and 4 (Fig. 13a). The slope of the bedrock profile beneath the M2 terrace is gentle, unlike its slope beneath the M1 terrace, because the former corresponds to the foreshore portion of the wave-cut platform whereas the latter probably corresponds to the inshore portion. Therefore, the shoreline angle of the bedrock profile must be between the core sites 4 and 5 along Section 5′. The inferred bedrock profile of the wave-cut platform corresponding to the M2 level and the slope behind it indicates that the elevation of the shoreline angle must be about 50 m a.s.l. (Fig. 13a). Thus, it is about 4–5 m lower than the inner edge of the M2 terrace surface. Shoreline angle is widely used as a sea-level indicator on rocky coasts without biological indicators (Pinter et al., 2001; Keller and Pinter, 2002), and it corresponds to mean higher high water (MHHW) or mean high water springs (MHWS) (Hull, 1987; ten Brink et al., 2006). Because the difference between MHHW and mean sea level (MSL) is only 0.5 m at Muroto Port (Japan Coast Guard, 2014), the shoreline angle can be considered to be equivalent to MSL during MIS 5c. Thus, the local uplift rate inferred from the elevation of the paleo-shoreline angle and the eustatic sea level during MIS 5c (94–100 ka) of −10 m (Siddall et al., 2006) was 0.60–0.64 m ky^{-1} (=60.0 m/94–100 ka).

Yoshikawa et al. (1964) previously reported the MIS 5c sea level in Section 5′, inferred from the elevation of the marine terrace surface, to

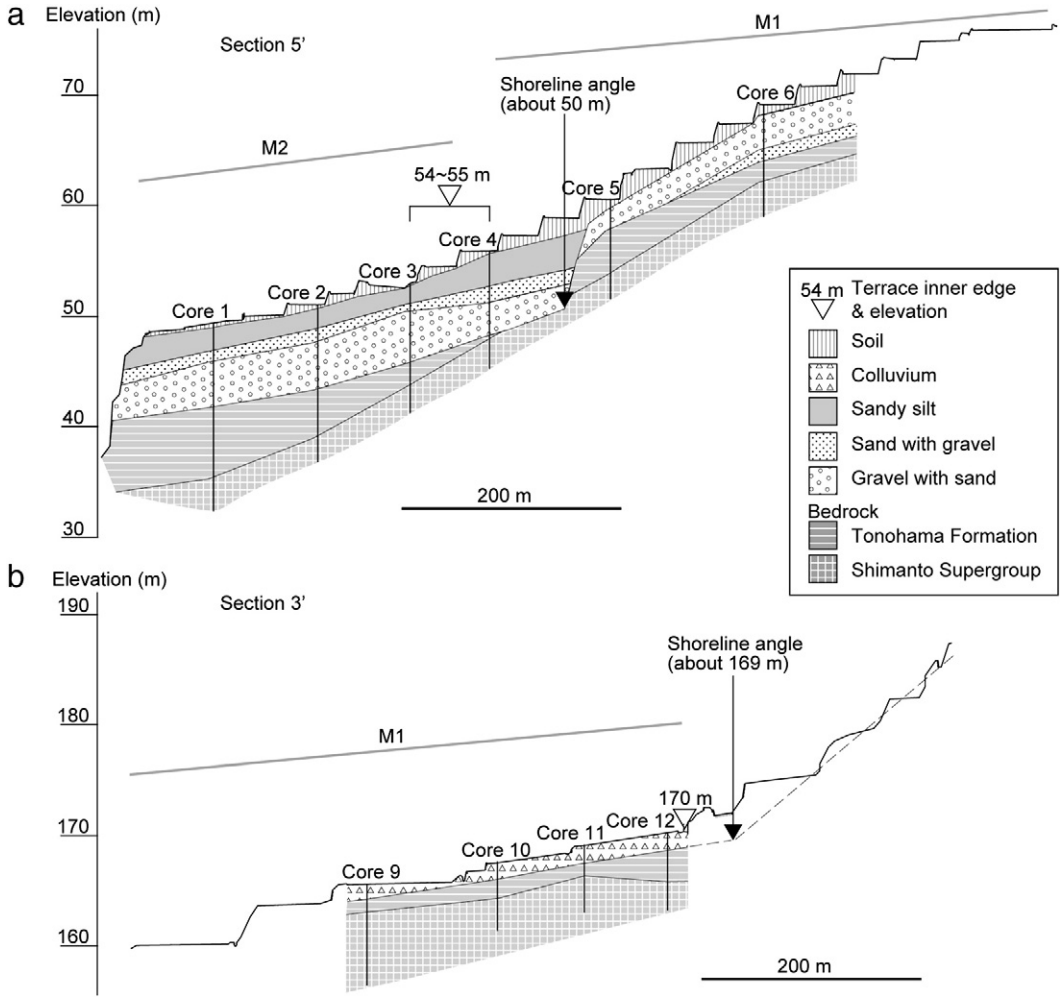

Fig. 13. Topographic and reconstructed geologic sections across the inner edge of terraces. Locations of the sections and coring sites in (a) Section 5′ and (b) Section 3′ are shown in Fig. 4e, c, respectively.

be at 54 m a.s.l., consistent with estimate of this study (54–55 m a.s.l.), and both estimates deviate less than 10% from the sea level estimated from the buried shoreline angle (50 m a.s.l.).

6.2. Buried shoreline angle beneath terrace M1

At Section 3′, the inner edge of the M1 terrace surface is at about 170 m a.s.l. (Figs. 4c; 13b), and the riser of an older terrace riser is just behind it. The four cores obtained from this section contain bedrock, colluvium, and soil in ascending order (Fig. 6). Thus, no terrace deposits, such as rounded gravel and sand, occur in these cores.

The bedrock surface in each of the Section 3′ cores was interpreted as the paleo-wave-cut platform corresponding to terrace M1, and the shoreline angle was estimated from the bedrock profile of the platform and the slope of the riser behind it to be at about 169 m a.s.l. (Fig. 13b). Thus, this paleo-sea level indicator is about 1.0 m below the inner edge of the M1 terrace surface. Then, the local uplift rate inferred from this elevation and the eustatic sea level during MIS 5e (116–132 ka) of 0–6 m (Siddall et al., 2006) is 1.28–1.51 m ky^{-1} (=169–175 m/116–132 ka).

Yoshikawa et al. (1964) previously reported the MIS 5e sea level at this location, inferred from the elevation of a marine terrace surface, to be 160 m a.s.l., somewhat lower than the estimate of this study (169 m a.s.l.). The published elevation was based on barometric altimetry, so it may have greater uncertainty than the estimates of this study.

7. Discussion

7.1. Uplift rates across the Muroto Peninsula and the mechanism of forearc deformation

To refine estimates of terrace deformation based on the elevations of the terrace inner edges, the elevation differences between the terrace inner edge and the buried shoreline angle of the M2 terrace in borehole cores along Section 5′ at Tosa-Tano (region 6) (Figs. 4e; 13a), and in the M1 terrace in borehole cores along Section 3′ at Nagano (region 5) (Figs. 4c; 13b), were determined.

In Section 5′, the inner edge of the M2 terrace is a depositional surface of sediments covering the wave-cut platform (Fig. 13a). The elevation difference between the terrace inner edge (54–55 m a.s.l.) and the buried shoreline angle (about 50 m a.s.l.) is 4–5 m. In Section 3′, the elevation difference between the inner edge of the M1 terrace (170 m) and the buried shoreline angle (about 169 m) is 1 m. The elevation difference in Section 3′ is smaller than the difference in Section 5′ because no gravel bed is present over the bedrock in Section 3′. Therefore, if a 5-m sediment cover is assumed to bury the shoreline angle, paleo-sea levels in the study area based on terrace inner edge elevations would be overestimated. That is, the shoreline angle in Section 3′ would be estimated to be at 165 m a.s.l. (170 m a.s.l.–5 m) rather than at its actual elevation (169 m a.s.l.), and the resulting uplift distribution would be in error (4 m, 2.4% [=(4/169) × 100] underestimated in this case). An overestimation of 5 m for the elevations of the M1 and M2 terrace inner edges

does not change the deformation patterns inferred from terrace inner edges (Fig. 12). However, it is necessary to consider the error in order to calculate the excess area of terrace deformation (see Section 7.2).

The anticlinal deformation inferred from the profile of terrace inner edges and buried shoreline angles is asymmetrical, with a narrow east-tilting forelimb and a wide west-tilting backlimb (Fig. 12). This pattern corresponds to the Muroto–Misaki anticline as documented in an offshore geologic profile (Okamura, 1990). The backlimb, including vertical offsets by the Gyodo-Zaki and Kiragawa faults, tilts westward as far as the boundary between regions 6 and 7 (Fig. 14b). The anticline is probably attributable to movement on the west-dipping Muroto–Misaki fault, which raises the backlimb owing to a bend (kink) in the buried fault at the boundary between regions 6 and 7; this movement may extend to the eastern edge of the Muroto–Misaki anticline on the seafloor (Fig. 2b).

The uplift in region 7, inferred from the inner edge elevations of the M1 and M2 terraces of 60 and 35 m a.s.l., respectively, is roughly constant (Fig. 12). This constant uplift is likely due to regional uplift of the Muroto Peninsula rather than to anticlinal deformation. Thus, the deformation of the Muroto Peninsula should be interpreted as a combination of regional uplift and anticlinal deformation. Furthermore, there is no evidence of tilting toward the arc interior (north-northwestward) during the Quaternary in the dips of marine sequences shown in seismic profiles (Okamura, 1990), so the regional uplift rate is probably uniform throughout the study area. In region 8, the elevations of the terrace inner edges may decrease westward, but for lack of data from the western side of region 8, it cannot be determined whether deformation in this area is local or regional. Therefore, the data from this section were not incorporated into the estimate of the regional uplift rate.

The calculated regional uplift rate of the Muroto Peninsula is 0.46 m ky^{-1} [=(60–3) m/124 ka] on the basis of the M1 terrace data (eustatic sea level of 0–6 m and MIS 5e age of 116–132 ka; Siddall et al., 2006). Similarly, the calculated rate is 0.46 m ky^{-1} [=(35 + 10) m/97 ka] on the basis of the M2 terrace data (eustatic sea level −10 m and MIS 5c age of 94–100 ka; Bassinot et al., 1994; Stirling et al., 1998). This rate for southwestern Japan is much higher

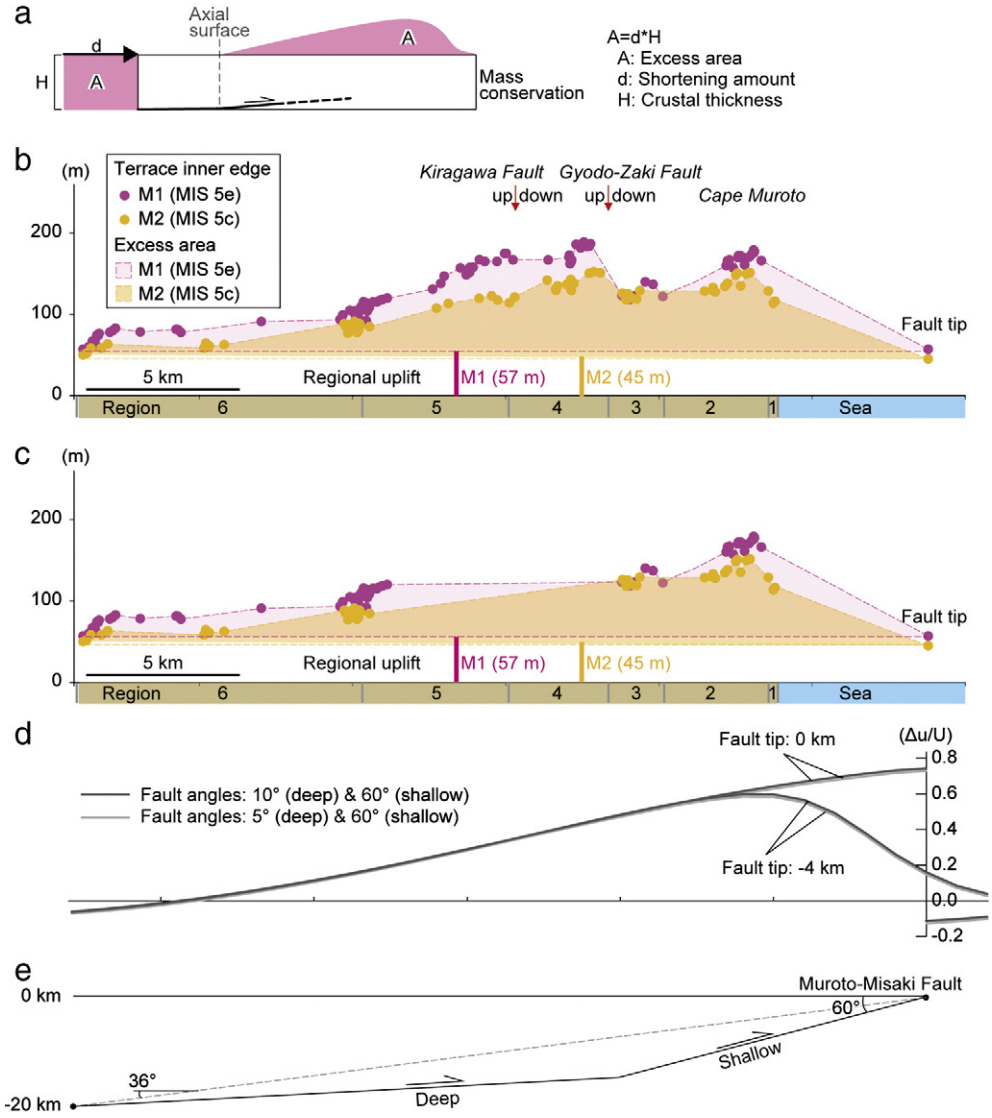

Fig. 14. Cross sections showing inferred late Pleistocene uplift of the Muroto Peninsula and a fault model of the Muroto–Misaki fault off Cape Muroto. (a) Schematic diagram showing how the shortening rate is determined by inference from the excess area defined by the profile of the shoreline angle using a mass-balance calculation (Chamberlin, 1910; Epard and Groshong, 1993; Bernard et al., 2007). (b) Uplift inferred from the inner edges of MIS 5e and 5c marine terraces. Fault tip, corresponding to the fault trace on the seafloor (Okamura, 1990), is 5 km east of the Muroto–Misaki anticline. (c) Uplift related to the Muroto–Misaki fault, estimated by subtracting the deformation on the Gyodo-Zaki and Kiragawa faults from the data of (b). (d) Vertical displacements of the ground surface in relation to fault depth. Vertical displacement (Δu) is normalized to the dip–slip of the fault (U). If the fault tip reaches the seafloor (0 km depth), the surface displacement increases toward the fault tip. If the fault tip lies beneath 4 km depth, displacement corresponds to an asymmetric anticline with its axis on Cape Muroto. (e) Geometry of the fault model.

than the rates of 0.1–0.3 m ky^{-1} (maximum rate is 0.36 m ky^{-1}) estimated across the central (Kesennuma–Isawa section) and northern (Shimokita Peninsula) parts of the northeastern Japan forearc (Matsu'ura et al., 2009, 2014a, 2014b). The tectonic setting of southwest Japan is a subduction zone dominated by sediment accretion, different from that of northeast Japan (an erosion-dominant subduction zone). In northeast Japan, the regional uplift may be due to isostatic compensation driven by crustal thickening (Matsu'ura et al., 2014b). In the Cascadia subduction zone (an accretion-dominant zone), in contrast, Brandon et al. (1998) interpreted the forearc uplift during the Quaternary to be driven by both accretion and within-wedge deformation. Therefore, in an accretion-dominant zone, the presence of thick sediments under the forearc may play an important role in causing high regional uplift rates.

7.2. Crustal shortening by an offshore fault and fault geometry

The shortening rate due to a blind thrust (d in Fig. 14a) can be calculated from the excess area of terrace deformation (A in Fig. 14a) and the vertical extent of the fault (H in Fig. 14a) by using a mass-balance calculation (Chamberlin, 1910; Epard and Groshong, 1993; Bernard et al., 2007). The excess areas of the M1 and M2 terraces are 1.755 and 1.494 km^2, respectively (Fig. 14b; Table 4). The fault is rooted at a depth of 20 km, the base of the crust (Kimura, 2001). The resulting shortening amounts since MIS 5e and 5c are 88 and 75 m, and their rates are 0.71 and 0.77 m ky^{-1}, respectively. Furthermore, the excess areas of just the Muroto–Misaki fault, estimated by subtracting the excess areas of the Gyodo-Zaki and Kiragawa faults from that of the Muroto Peninsula, are 1.493 and 1.369 km^2, and their shortening rates are 0.60 and 0.71 m ky^{-1}, respectively (Table 4). These rates are an order of magnitude smaller than the strike–slip rate on the Median Tectonic Line (7–9 m ky^{-1}; Research Group for Active Faults of Japan, 1991). The possible overestimation due to the estimated elevation error for terrace inner edges (5 m) would indicate a possible error in the shortening rates of about 10%.

To calculate the slip rate on a fault from the shortening rate, the fault's dip angle is required. Because there are no reliable data, such as from deep seismic profiles, for the fault dip angle in the study area, fault dip was estimated from other data. The distance between the fault tip on the seafloor and the northwestern end of the deformation area (region 6) is 27.6 km. The depth of the lower end of the fault is 20 km, given a crust thickness of 20 km (Kimura, 2001). A simple planar fault extending from this maximum depth to the fault tip, therefore, would have a dip angle of 36° (dashed line in Fig. 14e). However, such a low-angle fault is not in accordance with geomorphic traces on the seafloor (Okamura, 1990), which indicate high-angle faults. Further, to account for the uplift of the Muroto–Misaki anticline of 120 m, estimated by subtracting a regional uplift of 60 m from the total uplift since MIS 5e at Cape Muroto of 180 m, the Muroto–Misaki fault would need to have an implausible shortening rate. For example, an uplift rate of 1.0 m ky^{-1} (120 m/124 ka) on Cape Muroto requires a shortening rate of 1.38 m ky^{-1} on a fault with a 36° dip. However, the mass-balance calculation suggests that the shortening rate is just 0.60–0.71 m ky^{-1}. To explain the uplift of Cape Muroto since MIS 5e, a fault with 55–60° dip is required to cause an uplift of 1.0 m ky^{-1} at a shortening rate of 0.60–0.71 m ky^{-1}. Such a high-angle fault is in accordance with the seafloor geomorphology (Okamura, 1990). Thus, in this study the fault is modeled (Fig. 14e) as a single fault plane composed of deep and shallow segments with different dips. The shallow segment, which dips at 55–60°, probably rises from the deep segment to the west of the Muroto–Misaki anticline, but the depth of the intersection is not well constrained.

Vertical displacements were estimated by assuming a combined flat and ramp thrust fault model, characterized by gentle (5° or 10°) dips at depth and a steep (60°) dip in its shallow portion, by a dislocation calculation (Mansinha and Smylie, 1971). This calculation does not completely explain the amounts of permanent uplift of the Holocene and Pleistocene terraces, but it can constrain the geometry of the underlying fault as a first approximation (e.g., Benedetti et al., 2000; McCalpin and Carver, 2009). The magnitude of the vertical displacement differed, depending on whether a 5° or a 10° dip at depth was assumed, but the deformation patterns were similar (Fig. 14d). Displacements due to a uniform slip on the fault plane increase toward the fault tip, and they form an asymmetric anticline with its axis at the Muroto–Misaki anticline when the shallow fault tip is 4 km deep. In fact, the Muroto–Misaki fault reaches the seafloor (Okamura, 1990). Slip on the uppermost part of the shallow fault (0–4 km depth) should decrease toward the fault trace on the seafloor, but the paucity of data did not allow this factor to be considered in the dislocation calculation.

7.3. Estimation of fault location

This study modeled the Muroto–Misaki fault as a combined flat and ramp thrust across the Muroto Peninsula. Here the fault location is estimated by using the relationship between fault parameters and geologic evidence. At the Muroto–Misaki anticline, coseismic uplift of the L terraces inferred from sessile marine organisms was about 4 m at 1 ka and 2–3 m at 2.8 ka, respectively (Maemoku, 2001). Slip amounts on a shallow fault with a 60° dip (slip = uplift amount/sin 60°) during these 1 and 2.8 ka events would have been 4.6 and 2.3–3.5 m, respectively. Published relationships between displacement and fault length and earthquake magnitude for reverse faults (Wesnousky, 2008) suggest that these slip amounts resulted from a fault rupture length (magnitude) of 77 km (M_w = 7.7) for the 1 ka event and of 38–58 km (M_w = 7.1–7.4) for the 2.8 ka event. Although the data set of Wesnousky (2008) is for ruptures that were not blind thrusts, it allows rough estimation of the Muroto–Misaki fault's length and location relative to the Muroto Peninsula.

Because geologic evidence shows that the Muroto–Misaki anticline plunges southward (Okamura, 1990), the Muroto–Misaki fault does not extend southward beyond the anticline but it may extend north of Cape Muroto (Fig. 15). The magnitude of such a prolongation is unclear in the absence of marine terrace deformation measurements. However, the bedrock (Shimanto Supergroup) along the northward extension of the Muroto–Misaki fault is severely deformed by the Muroto Flexure (DiTullio and Byrne, 1990; Hibbard and Karig, 1990). This flexure, which has a N–S or NNW–SSE trending axis, is traceable to about 35 km north of Cape Muroto and is attributed to subduction of a spreading ridge prior to the Quaternary (Hibbard and Karig, 1990). Moreover, the flexure forms an asymmetrical anticline, with a narrow east-tilting forelimb and a wide west-tilting backlimb (DiTullio, 1989), similar to the Muroto–Misaki anticline. This bedrock structure is likely to be

Table 4
Parameters for the mass-balance calculation and results.

Case	Terrace	Sea level (m)	Excess area (km^2)	Crust thickness (km)	Shortening amount (m)	Terrace age (ka)	Shortening rate (m ky^{-1})
1: Muroto–Misaki, Gyodo–Zaki, and Kiragawa faults	M1	3	1.755	20	88	124	0.71
	M2	−10	1.494	20	75	97	0.77
2: Muroto–Misaki fault	M1	3	1.493	20	75	124	0.60
	M2	−10	1.369	20	68	97	0.71

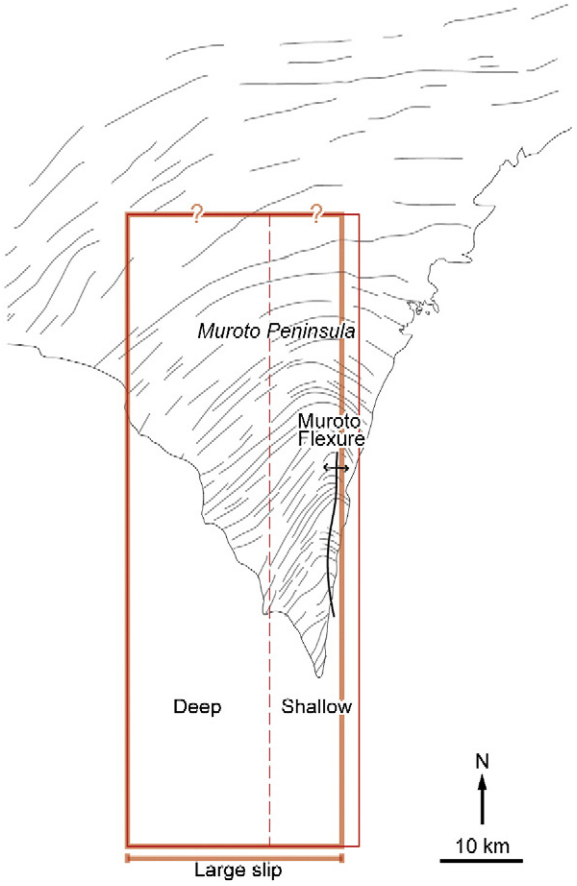

Fig. 15. Map showing the estimated location of the Muroto–Misaki fault. The fault length of 58 km is based on the relation between displacement and fault length of Wesnousky (2008) (see text). Trends of strata (gray lines) and the trace of the Muroto Flexure are from Hibbard and Karig (1990) and DiTullio and Byrne (1990), respectively.

reactivated under the Quaternary tectonic setting of arc-parallel compression due to the oblique subduction of the Philippine Sea plate. Thus, the fault model proposed in this study can reasonably explain both terrace deformation (a proxy for growth strata) and bedrock deformation (pre-growth strata), but this fault model should be improved by further study.

8. Conclusions

The recent deformation of the southwest Japan forearc, the overriding plate in the southwest Japan subduction zone, was inferred from elevation data of the inner edges of dated marine terrace surfaces. More accurate uplift rates were also derived from elevations of the buried shoreline angles beneath the MIS 5c and 5e marine terrace surface at two places on the Muroto Peninsula. The conclusions are as follows:

(1) Six terrace surfaces were classified. In ascending order they are named, L, M3, M2, M1, H2, and H1. L is a Holocene terrace group and M3 comprises local fluvial surfaced along rivers. The M2 and M1 terraces were correlated with MIS 5c and 5e, respectively, from the stratigraphic positions of tephras K-Tz (MIS 5c–5b) and Aso-4 (MIS 5b), and H2 was correlated with MIS 7, the highstand previous to MIS 5e.

(2) The profile of uplift across the Muroto Peninsula inferred from inner edge elevations of the M1 terrace surface shows a generally decreasing uplift rate northwestward from 1.2–1.6 m ky^{-1} on Cape Muroto to 0.3–0.7 m ky^{-1} at the northwest end of the Muroto Peninsula, though this trend is interrupted by vertical offsets by the Gyodo-Zaki and Kiragawa faults.

(3) The buried shoreline angle is a more accurate uplift indicator. This indicator is at 50 m a.s.l. for terrace M2, 4–5 m below the terrace inner edge, as determined by reconstructing the bedrock profile of the paleo-sea cliff and buried wave-cut platform in the Tosa-Tano area. For terrace M1, the buried shoreline angle is at 169 m a.s.l., 1 m below the terrace inner edge, in the Nagano area. Thus, the overestimation of terrace elevations due to the reliance on terrace inner edge elevations is probably 5 m or less in the study area.

(4) The vertical deformation across the Muroto Peninsula during the late Quaternary is consistent with fault-related folding by the offshore Muroto–Misaki fault.

(5) The regional uplift of 0.46 m ky^{-1} was likely driven by sediment accretion along the southwest Japan subduction zone and within-wedge deformation, and the residual uplift rate (about 1 m ky^{-1}) on the Muroto–Misaki anticline is interpreted as local anticlinal deformation by an offshore fault.

(6) A mass-balance calculation based on excess area represented by terrace deformation and fault-related folding yielded a shortening rate of 0.71–0.77 m ky^{-1} in the study area. The shortening rate on just the Muroto–Misaki fault, estimated by subtracting the excess areas of other local faults, is 0.60–0.71 m ky^{-1}.

(7) The proposed fault model for the Muroto–Misaki fault, a composite flat (5–10° dip) and ramp (60° dip) thrust fault, explains the shortening rate and uplift rate since MIS 5e. A northern extension of the fault probably corresponds to the Muroto Flexure identified in bedrock mapping.

Acknowledgments

I thank K. Takada and H. Kinoshita (Fukken Consultants) for their help with terrace mapping and coring, and A. Furusawa for chemical analyses. I also thank T. Komatsubara (Geological Survey of Japan) for his help in the dislocation calculation, which included the use of his coding. I benefited from the comments of T. Oguchi (Editor in Chief of Geomorphology), F. Gutierrez (Universidad de Zaragoza), G. Botha (Council for Geoscience), N. Hamada (formerly JNES), K. Shimazaki (formerly NRA), M. Miyawaki and K. Sugaya (S/NRA/R), and N. Goto and K. Ichikawa (Hanshin Consultants), which improved the manuscript. Some figures were prepared with Generic Mapping Tools version 4.2.0 (Wessel and Smith, 1998).

References

Ando, M., 1975. Source mechanism and tectonic significance of historical earthquakes along the Nankai Trough, Japan. Tectonophysics 27, 119–140.
Aoki, K., 2008. Revised age and distribution of ca. 87 ka Aso-4 tephra based on new evidence from the northwest Pacific Ocean. Quat. Int. 178, 100–118.
Bassinot, F.C., Labeyrie, L.D., Vincent, E., Quidelleur, X., Shackleton, N.J., Lancelot, Y., 1994. The astronomical theory of climate and the age of the Brunhes–Matuyama magnetic reversal. Earth Planet. Sci. Lett. 126, 91–108.
Benedetti, L., Tapponier, P., King, G.C.P., Meyer, B., Manighetti, I., 2000. Growth folding and active thrusting in the Montello region, Vento, northern Italy. J. Geophys. Res. 105, 739–766.
Bernard, S., Avouac, J.P., Dominguez, S., Simoes, M., 2007. Kinematics of fault-related folding derived from a sandbox experiment. J. Geophys. Res. 112, B03S12. http://dx.doi.org/10.1029/2005JB004149.
Brandon, M.T., Roden-Tice, M.K., Garver, J.I., 1998. Late Cenozoic exhumation of the Cascadia accretionary wedge in the Olympic Mountains, northwest Washington State. Geol. Soc. Am. Bull. 110, 985–1009.
Central Disaster Prevention Council, 2013. Hazard assumption of large earthquake along the Nankai Trough. http://www.bousai.go.jp/jishin/nankai/nankaitrough_info.html (in Japanese).
Chamberlin, R.T., 1910. The Appalachian folds of central Pennsylvania. J. Geol. 27, 228–251.
Cronin, S.J., Neall, V.E., Stewart, R.B., Palmer, A.S., 1996. A multiple-parameter approach to andesitic tephra correlation, Ruapehu volcano, New Zealand. J. Volcanol. Geotherm. Res. 72, 199–215.
DiTullio, L., 1989. Development of the Shimanto belt (Eocene) on the Muroto Peninsula, southeastern Shikoku. Earth Monthly 11, 673–678 (in Japanese).

DiTullio, L., Byrne, T., 1990. Deformation paths in the shallow levels of an accretionary prism: The Eocene Shimanto belt of southwest Japan. Geol. Soc. Am. Bull. 102, 1420–1438.
Epard, J.L., Groshong, R.H., 1993. Excess area and depth to detachment. AAPG Bull. 77, 1291–1302.
Fitch, T.J., 1972. Plate convergence, transcurrent faults and internal deformation adjacent to southeast Asia and the western Pacific. J. Geophys. Res. 77, 4432–4460.
Furusawa, A., 2003. Correlation, age, and source of Yumuta tephra around Yufudake volcano. Bull. Volcanol. Soc. Jpn. 48, 309–319 (in Japanese, with English Abstr).
Furusawa, A., Nakamura, C., 2009. Method for the identification of the K-Tz tephra based on a detailed comparison of major elements within glass inclusions in tephra quartz. J. Geol. Soc. Jpn. 115, 544–547 (in Japanese, with English Abstr).
Headquarter of Earthquake Research Project, 2013. Long-term activity evaluation of seismicity along the Nankai Trough (second version). http://www.jishin.go.jp/main/chousa/13may_nankai/nankai2_setsumei.pdf (in Japanese).
Hibbard, J.P., Karig, D.E., 1990. Structural and magmatic responses to spreading ridge subduction zone: an example from southwest Japan. Tectonics 9, 207–230.
Hull, A.G., 1987. A late Holocene marine terrace on the Kidnappers coast, North Island, New Zealand. Quat. Res. 28, 183–195.
Iwai, M., Kondo, Y., Kikuchi, N., Oda, M., 2006. Overview of stratigraphy and paleontology of Pliocene Tonohama Group, Kochi Prefecture, southwest Japan. (supplement), J. Geol. Soc. Jpn. 112, 27–40 (in Japanese, with English Abstr).
Japan Coast Guard, 2014. Tables of tidal harmonic constant. http://www1.kaiho.mlit.go.jp/KAN5/siryouko/monosiri/tyouseki2.htm (in Japanese).
Kamata, H., Hoshizumi, H., 1996. Pyroclastic fall deposits originated from Kuju volcano and widespread tephras. Japan Association for Quaternary Research. Inventory of Quaternary Outcrops—Tephra in Japan. Japan Association for Quaternary Research, Tokyo, p. 299 (in Japanese).
Kamata, H., Danhara, T., Itoh, J., Hoshizumi, H., Watanabe, Y., 1998. Fission-track ages of zircons in the Miyagi, Shimosaka and Handa pyroclastic-flow deposits erupted from Kuju volcano in central Kyushu, Japan. Bull. Volcanol. Soc. Jpn. 43, 69–73 (in Japanese).
Kanaya, A., 1978. Holocene marine terraces and tectonic movements of the Muroto Peninsula. Geogr. Rev. Jpn. 51, 451–463 (in Japanese).
Kawai, S., Miyake, Y., 1999. Grain-size and mineral compositions of Aira-Tn tephra, Japan — an example of the lateral variations of wide-spread tephra. J. Geol. Soc. Jpn. 105, 597–608 (in Japanese, with English Abstr).
Kawamura, N., 2009. Stratigraphy of the late Pleistocene and Holocene sediments associated with correlation of some tephra beds in the Matsuyama Plain, Ehime prefecture, southwest Japan. Quat. Res. (Jpn.) 48, 379–394 (in Japanese, with English Abstr).
Keller, E.A., Pinter, N., 2002. Active Tectonics: Earthquakes, Uplift, and Landscape. Second ed. Prentice Hall (362 p.).
Kimura, J., 1996. Takano Formation at Shinko town, Nagano city — sediments including wide spread tephras of the last 130 ka. In: Japan Association for Quaternary Research (Ed.), Inventory of Quaternary Outcrops — Tephra in Japan. Japan Association for Quaternary Research, Tokyo, pp. 34–35 (in Japanese).
Kimura, S., 2001. Some characteristics of seismic activities in and around Shikoku in relation to the 1946 Nankai earthquake. J. Geogr. 110, 581–591 (in Japanese, with English Abstr).
Kimura, G., 2002. Tectonics of Convergent Plate Boundaries. University of Tokyo Press, Tokyo (271 p. in Japanese).
Atlas of Quaternary Marine Terraces in the Japanese Islands. In: Koike, K., Machida, H. (Eds.), University of Tokyo Press, Tokyo (105 pp., in Japanese, with English Abstr).
Kumahara, Y., Nagaoka, S., 2002. Identification of the Kuju-Daiichi Tephra Layer, and the age of the late Pleistocene fluvial terrace along the Matsuda River in southwestern Shikoku, Japan. Quat. Res. (Jpn.) 41, 213–219 (in Japanese with English Abstr).
Lave, J., Avouac, J.P., 2000. Active folding of fluvial terraces across the Siwalik hills, Himalayas of central Nepal. J. Geophys. Res. 105, 5735–5770.
Lay, T., Kanamori, H., Ammon, C.J., Nettles, M., Warc, S.N., Aster, R.C., Beck, S.L., Bilek, S.L., Brudzinski, M.R., Butler, R., DeShon, H.R., Ekstrom, G., Satake, K., Sipkin, S., 2005. The great Sumatra–Andaman earthquake of 26 December 2004. Science 308, 1127–1133.
Lowe, D.J., 2011. Tephrochronology and its application: a review. Quat. Geochronol. 6, 107–153.
Machida, H., Arai, F., 2003. Atlas of Tephra in and Around Japan. University of Tokyo Press, Tokyo (336 pp. in Japanese, with English Abstr).
Maemoku, H., 1988. Holocene crustal movement in Muroto Peninsula, southwest Japan. Geogr. Rev. Jpn (Ser. A) 61, 747–769 (in Japanese, with English Abstr).
Maemoku, H., 1996. Marine terrace deposits of the Murotomisaki surface in Kochi prefecture. In: Japan Association for Quaternary Research (Ed.), Inventory of Quaternary Outcrops — Tephra in Japan. Japan Association for Quaternary Research, Tokyo (292 pp. in Japanese).
Maemoku, H., 2001. Reexamination of coseismic uplift of Cape Muroto, southwest Japan, using AMS ^{14}C ages of raised sessile organisms. J. Geogr. 110, 479–490 (in Japanese, with English Abstr).
Maemoku, H., 2006. Quaternary crustal movement and coseismic uplift along Muroto Peninsula. (supplement), J. Geol. Soc. Jpn. 112, 17–26 (in Japanese, with English Abstr).
Mansinha, L., Smylie, D.E., 1971. The displacement fields of inclined faults. Bull. Seismol. Soc. Am. 61, 1433–1440.
Matsu'ura, T., Kimura, H., 2010. Late Quaternary crustal shortening rate across the Shinjo basin, northeast Japan. J. Geophys. Res. 115, B11409. http://dx.doi.org/10.1029/2009JB006963.
Matsu'ura, T., Furusawa, A., Saomoto, H., 2009. Long-term and short-term vertical velocity profiles across the forearc in the NE Japan subduction zone. Quat. Res. 71, 227–238.
Matsu'ura, T., Ueno, T., Furusawa, A., 2011. Characterization and correlation of cryptotephras using major-element analyses of melt inclusions preserved in quartz in last interglacial marine sediments, southeastern Shikoku, Japan. Quat. Int. 246, 48–56.
Matsu'ura, T., Furusawa, A., Shimogama, K., Goto, N., Komatsubara, J., 2014a. Late Quaternary tephrostratigraphy and cryptotephrostratigraphy of deep-sea sequences (Chikyu C9001C cores) as tools for marine terrace chronology in NE Japan. Quat. Geochronol. 23, 63–79.
Matsu'ura, T., Kimura, H., Komatsubara, J., Goto, N., Yanagida, M., Ichikawa, K., Furusawa, A., 2014b. Late Quaternary uplift rate inferred from marine terraces, Shimokita Peninsula, northeastern Japan: a preliminary investigation of the buried shoreline angle. Geomorphology 209, 1–17.
McCaffrey, R., 1992. Oblique plate convergence, slip vectors, and forearc deformation. J. Geophys. Res. 97, 8905–8915.
McCalpin, J.P., Carver, G.A., 2009. Paleoseismology of compressional tectonic environments. In: McCalpin (Ed.), Paleoseismology, Second ed. International Geophysics 95. Elsevier, Oxford, pp. 315–419. http://dx.doi.org/10.1016/S0074-6142(09)95005-7.
Morie, T., Ozawa, H., Okumura, K., 2001. Description and correlation of the Nagate tephra in the terrace deposits at the southern foot of Asan range in Tokushima prefecture, southwestern Japan. Quat. Res. (Jpn.) 40, 331–336 (in Japanese with English Abstr).
Okal, E.A., 2007. Seismic records of the 2004 Sumatra and other tsunamis: a quantitative study. Pure Appl. Geophys. 164, 325–353.
Okamura, Y., 1990. Geologic structure of the upper continental slope off Shikoku and Quaternary tectonic movement of the outer zone of southwest Japan. J. Geol. Soc. Jpn. 96, 223–237 (in Japanese, with English Abstr).
Okamura, Y., Kamishima, M., 1986. Geological Map Off Muroto Zaki and Explanatory Notes 1:200,000. Geological Survey of Japan, Tokyo (31 p. with 4 sheets (in Japanese)).
Okuno, M., Nakamura, T., Kamata, H., Ono, K., Hoshizumi, H., 1998. AMS ^{14}C age of the Handa pyroclastic-flow deposit from Kuju volcano, Japan. Bull. Volcanol. Soc. Jpn. 43, 75–79 (in Japanese).
Ono, K., 1996. Aso-4 pyroclastic deposits on southwest slope of Kuju volcano. In: Japan Association for Quaternary Research (Ed.), Inventory of Quaternary Outcrops — Tephra in Japan. Japan Association for Quaternary Research, Tokyo, p. 33 (in Japanese).
Pinter, N., Johns, B., Little, B., Vestal, W.D., 2001. Fault-related folding in California's Northern Channel Islands documented by rapid-static GPS positioning. GSA Today 11, 4–9.
Plafker, G., 1972. Alaskan earthquake of 1964 and Chilean earthquake of 1960: implications for arc tectonics. J. Geophys. Res. 77, 901–925.
Plafker, G., 1987. Application of marine-terrace data to paleoseismic studies. In: Crone, A.J., Omdahl, E.M. (Eds.), Directions in Paleoseismology. United States Geological Survey Open File Report 87-673, pp. 146–156.
Research Group for Active Faults of Japan, 1991. Active Faults in Japan: Sheet Maps and Inventories (revised edition). University of Tokyo Press, Tokyo (437 pp. in Japanese with English abstr).
Seno, T., Sakurai, T., Stein, S., 1996. Can the Okhotsk plate be discriminated from the North American plate? J. Geophys. Res. 101 (B5), 11,305–11,315. http://dx.doi.org/10.1029/96JB00532.
Siddall, M., Chappell, J., Potter, E.-K., 2006. Eustatic sea level during past interglacials. In: Sirocko, F., Claussen, M., Sanchez Goñi, M.F., Litt, T. (Eds.), The Climate of Past Interglacials. Elsevier, Amsterdam, pp. 75–92.
Stirling, C.H., Esat, T.M., Lambeck, K., McCulloch, M.T., 1998. Timing and duration of the last interglacial: evidence for a restricted interval of widespread coral reef growth. Earth Planet. Sci. Lett. 160, 745–762.
Suppe, J., 1983. Geometry and kinematics of fault-bend folding. Am. J. Sci. 283, 684–721.
Taira, A., Tashiro, M., Okamura, M., Katto, J., 1980. The geology of the Shimanto Belt in Kochi Prefecture, Shikoku, Japan. In: Taira, A., Tashiro, M. (Eds.), Geology and Paleontology of the Shimanto Belt: Kochi. Rinya-Kosakai Press, Tokyo, Japan, pp. 319–389.
ten Brink, U.S., Song, J., Bucknam, R.C., 2006. Rupture models for the A.D. 900–930 Seattle fault earthquake from uplifted shorelines. Geology 34, 585–588.
Wesnousky, S.G., 2008. Displacement and geometrical characteristics of earthquake surface ruptures: issues and implications for seismic hazard analysis and the process of earthquake rupture. Bull. Seismol. Soc. Am. 98, 1609–1632.
Wessel, P., Smith, W.H.F., 1998. New, improved version of the Generic Mapping Tools released. Eos. Trans. AGU 79, 579.
Yonekura, N., 1975. Quaternary tectonic movements in the outer arc of southwest Japan with special reference to seismic crustal deformation. Bull. Dep. Geogr. Univ. Tokyo 15, 47–62.
Yoshikawa, T., Kaizuka, S., Ota, Y., 1964. Mode of crustal movement in the late Quaternary on the southeast coast of Shikoku, southeastern Japan. Geogr. Rev. Jpn. 37, 627–648 (in Japanese, with English Abstr).